The M_2 tide in the Mediterranean Sea: dynamic analysis and data assimilation

PRIMO-0
Tide
Semi-enclosed basin mode
Mediterranean circulation
Data assimilation

PRIMO-0
Marée
Mer semi-fermée
Circulation en Méditerranée
Assimilation de données

Carlos J. LOZANO[a] and Julio CANDELA[b]

[a] Department of Earth Sciences, 185 Pierce Hall, Harvard University, Cambridge, Massachusetts 02138, USA.

[b] Department of Physical Oceanography, Woods Hole Oceanographic Institution Woods Hole, Massachusetts 02543, USA.

Received 10/05/94, in revised form 28/02/95, accepted 02/03/95.

ABSTRACT

The predominant M_2 tide in the Mediterranean Sea is examined using the linearized Laplace tidal equations including the astronomical gravitational potential, the Atlantic tide entering through the Strait of Gibraltar, the Earth tide, the effects of the Earth deformation due to the ocean tide load and bottom friction. The model solution is based on a decomposition of the primitive variables in terms of basis functions associated to the Helmholtz-Proudman potentials.

The net tidal power input into the basin is 1.63 10^8 W. Bottom friction dissipation accounts for –0.94 10^8 W. The work done by the bottom deformation due to global (–0.62 10^8 W) and local (–0.07 10^8 W) tide load effects extract energy from the system. The net energy flux into the basin through the Strait of Gibraltar (6.52 10^8 W) is four times larger than the net power input, but the astronomical tidal body forces operating over the interior of the basin do work in opposition, implying a net power extraction of –4.89 10^8 W.

In addition to the Helmholtz mode with a period of 5.3 days, the normal modes contributing to the M_2 tide have periods between 8 h and 32 h. These modes are associated to regional sea level and transport structures in the Gulf of Gabes (8.2 h), the Adriatic and Aegean Seas (12.0 h) and basin-wide features in the Eastern and Western basins (1.3 d).

Sixty tide-gauge stations inside the Mediterranean Sea, together with transport measurements through the Strait of Gibraltar, are used to calibrate the model. Comparison of the data and the unconstrained dynamic model sea-surface height shows a rms difference of 4.5 cm. Allowing for errors in the model and the observations and selecting the magnitude of the error in the model (32 %), a robust estimate of the basin response yields a rms difference of 2.5 cm with the observations.

RÉSUMÉ

La marée M_2 en Méditerranée : analyse dynamique et assimilation de données.

La composante dominante M_2 de la marée en mer Méditerranée est étudiée à l'aide des équations de Laplace, lesquelles incluent le potentiel astronomique gravitationnel, la marée Atlantique pénétrant le détroit de Gibraltar, la marée terrestre, les effets de la déformation de la Terre causés par la charge due aux marées océaniques et la friction sur le fond marin. Le problème est résolu à

l'aide d'une décomposition des variables primitives sur les fonctions de base associées aux potentiels de Helmholtz-Proudman.
La puissance nette totale injectée dans le bassin méditerranéen par la marée est de 1,63 10^8 W. La puissance dissipée par la friction sur le fond est de –0,94 10^8 W. Le reste est absorbé par la déformation du fond causée par la charge de la marée globale (–0,62 10^8 W) et la marée locale (–0,07 10^8 W). Le flux net d'énergie pénétrant le bassin à travers le détroit de Gibraltar (6,52 10^8 W) est quatre fois plus élevé que la puissance nette totale injectée, mais est en partie compensé par le forçage astronomique des marées à l'intérieur du bassin, ce qui implique une puissance nette extraite de –4,89 10^8 W.
En plus du mode de Helmholtz qui a une période de 5,3 jours, les modes normaux contribuant à la marée M_2 ont des périodes comprises entre 8 h et 32 h. Ces modes sont associés au niveau régional de la mer et aux transports causés par les marées dans le Golfe de Gabès (8,2 h), l'Adriatique et la Mer Egée (12,0 h), et aux caractéristiques globales des bassins oriental et occidental (1,3 j).
Le modèle est calibré à l'aide de données provenant de soixante marégraphes en Mer Méditerranée et de mesures des flux dans le Détroit de Gibraltar. Une comparaison des données et de l'élévation du niveau de la mer prédite par le modèle dynamique en l'absence de contraintes, indique un écart-type de 4,5 cm. Prenant en compte les erreurs associées au modèle (32 %) ainsi que les erreurs associées aux observations, une estimation de la réponse du bassin indique un écart-type de 2,5 cm entre le modèle et les observations.

Oceanologica Acta, 1995, **18**, 4, 419-441

INTRODUCTION

The Mediterranean Sea is a semi-enclosed basin connected to the Atlantic Ocean through the Strait of Gibraltar. The basin (Fig. 1) has a complex topography with deep basins separated by sills and islands, and circumvented for the most part by narrow shelves. Important exceptions are the Tunisian shelf and the relatively shallow Adriatic and Aegean Seas. The Mediterranean basin itself can be seen as a composite of semi-enclosed basins, the largest being the Western and Eastern basins separated by the Straits of Sicily and Messina. This complex topography is reflected in the dynamic structures supported by the basin.

The predominant tidal signal in the Mediterranean Sea is the M_2 tide, and for this constituent a detailed analysis is carried out in terms of the forced linearized Laplace equations. The body forces considered are the gravitational attraction of the Moon and Sun and the gravitational deviations induced by Earth deformations. Account is taken of bottom friction and bottom deformations. The gravitational deviations and the bottom deformations are due both to the Earth tide and to the ocean tidal load.

To set the approach taken in this study in context, a brief summary of our present knowledge on the dynamics of the response to tidal forcing follows. Early studies which explained the tides in the Mediterranean using gravitational theories were reviewed by Grace (1931). Most of these studies considered the equilibrium tide, or small departures from it, as the main forcing applied to either a closed Mediterranean basin or a basin influenced by the Atlantic tide. Subsequently, further dynamics were introduced assuming a basin composed of one-dimensional narrow non-rotating channels. On the basis of these and other *ad hoc* assumptions, the observational data for the M_2 tide were interpreted by Defant (1961) as a set of standing waves in the Western and Eastern basins with amphidromes southeast of the Balearic Islands, at the Strait of Sicily and south of Crete. The Aegean was assumed to co-oscillate with the Levantine basin, with a nodal line between Crete and Rhodes. The Adriatic co-oscillation with the Ionian had an amphidromic point near its present estimated location. Models with more or less topographic detail were constructed for the Western basin, the Ionian-Levantine basin and the Adriatic and the Aegean basins, considering them as closed or driven at the boundaries (co-oscillations). The model predictions show a good qualitative agreement with the tide gauge data available at the time. These studies brought to the fore the importance of the natural modes of the basin and their co-oscillations with other basins in the tidal response [see, for instance, Defant (1961) in relation to the Defant (1914) and Sterneck (1914, 1919) studies of the Adriatic Sea]. These developments practically ceased in the mid-1950s. Some issues, such as the role of the co-oscillating Atlantic tide, remained controversial (Maloney and Burns, 1958; Lacombe, 1961). For a comprehensive review of this period, see Defant (1961) and Elliott (1993).

A new impetus in the study of the tides came about with the ability to perform the computations required by two-dimensional dynamic models (Platzman, 1972; Platzman, 1978; Accad and Pekeris, 1978), and later with the availability of altimetric data. The first basin-wide numerical study of the tide was done by Dressler (1980). Schwab and Rao (1983) constructed a set of gravitational normal modes using the formulation of Proudman (1938) for a closed

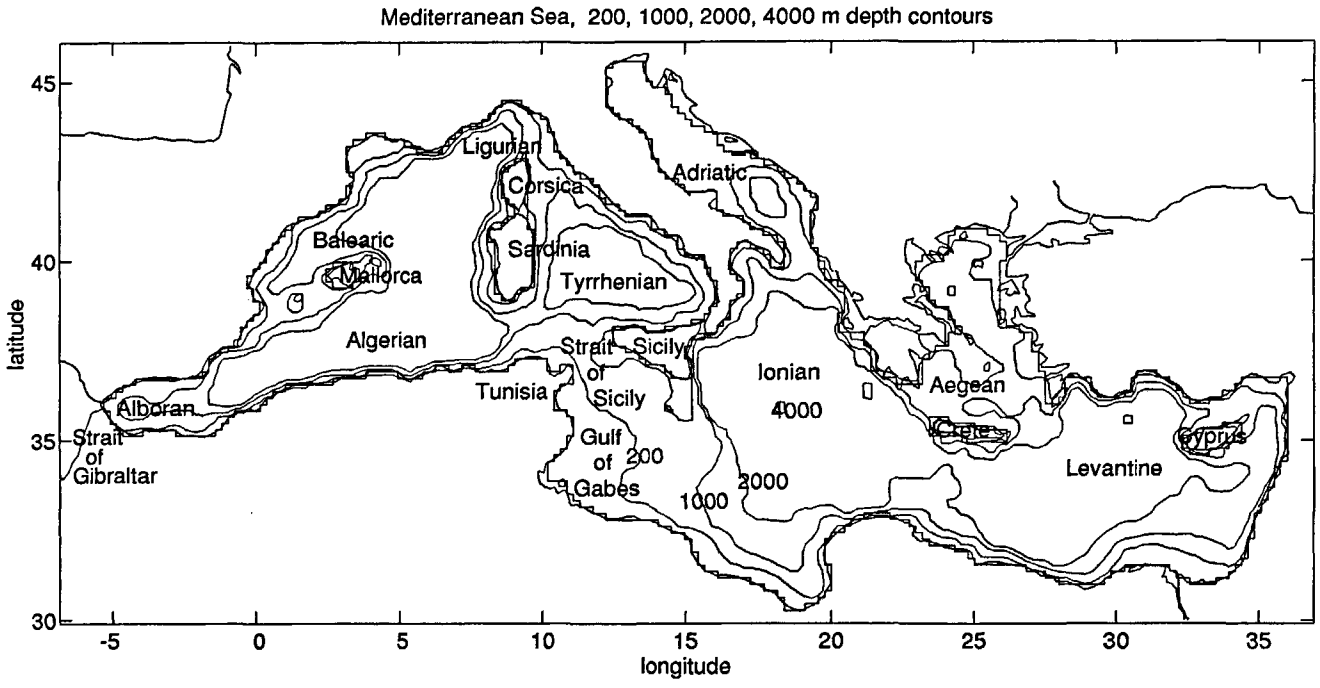

Figure 1

Mediterranean Sea bathymetry showing depth contours at 0, 200, 1000, 2000 and 4000 m. The step-like polygonal lines are the boundaries of the model grid. The model grid spacing is uniformly 20 km along both latitude and longitude. The multiply-connected discrete domain resolves four islands corresponding to Majorca, Corsica-Sardinia, Crete, and Cyprus. Sicily is considered attached to the rest of Italy.

Mediterranean Sea, without the Adriatic and the Aegean basins, and ignoring circulation conditions. Recently Canceill *et al.* (1994) have applied Le Provost's finite element numerical model to the entire basin with a nominal resolution of about 15 km, and constructed co-tidal charts for nine of the principal tidal constituents. The tides predicted by this model, constrained with tide gauge observations at selected points, compare well with the remaining tide gauge data. In these authors' formulation, non-linear terms are included. Finally, regional tidal models for the Aegean Sea (Livieratos and Zadro, 1977) and for the Strait of Sicily and the Tunisian Shelf (Mosetti and Purga, 1985; Molines, 1992) have provided a detailed structure of the important constituents at these locations.

The phenomenology of the tides in the Mediterranean deduced from tide gauges was lucidly synthesized by Villian (1949, 1952). Since that time, the collection and refinement of tidal constants from tidal gauges has continued (Purga *et al.*, 1979; Mosetti, 1989). The Geosat altimetric data, processed by the along-track differencing method, was used by Cartwright and Ray (1990) to obtain global maps of the tides including the Mediterranean Sea. Later, Sanchez, Ray and Cartwright (1992) used Proudman functions as interpolating functions with a 0.5 degree resolution to meld tide gauge and Geosat data.

The approach to the dynamic response to tidal forcing adopted in this paper is described here, and in greater detail in the methods section below. The tidal forced problem is defined in terms of the forced linearized Laplace tidal equations in the frequency domain. The traditional equations are extended to include circulation conditions around islands, and the interaction through the Strait of Gibraltar with the Atlantic Ocean. The inclusion of the ocean tidal load effects yields an integro-differential equation (Hendershott, 1972) for the spatial variables in the basin.

The method used to treat the spatial components comprises a spectral approximation which first involves the expansion of the sea surface height, the divergence of the transport and the relative vorticity of the vertically-averaged horizontal velocity in terms of basis functions constructed from the eigenfunctions of the Helmholtz-Proudman potentials (Proudman, 1938). The basis functions are defined over a discrete grid (20-km nominal grid spacing) using a realistic topography derived from the ETOPO5 data set of NOAA. The boundary of the discrete grid and the bottom relief are shown in Figure 1. The second step in the spectral method involves the projection of the equations of mass continuity, divergence and vorticity on to the appropriate basis functions, taking due account of the circulation conditions around islands and the continuity of transport and pressure across the Strait of Gibraltar. The result of these projections is an algebraic system of equations for the coefficients of the series expansions of the velocity potentials and the sea surface elevations. The algebraic system of equations represents the internal dynamics of the basin and its interaction with the open ocean. The interest here is to resolve the spatial scales contributing to the basin- and sub-basin scale tidal interactions. Non-linear effects are observed to be active in limited and relatively small-scale regions in the basin, *e.g.* the Strait of Messina. Here we assume that the large-scale response is essentially well represented with linear dynamics.

The normal modes of the semi-enclosed basin, as well as the average power exchanged during a tidal cycle by the different components of the system, are readily deduced

from this algebraic system of equations. A sensitivity analysis of the number of terms in the series representation (not shown here) indicates that stable and accurate normal modes pertinent to the tidal regime are obtained with about 500 degrees of freedom. This implies a substantial collapse from the initial number of degrees of freedom available in the model representation (~ 17 000), as well as a significant reduction in the numerical complexity of the problem.

The model tuning was limited to small changes in the geometrical parameters describing the Strait of Gibraltar and in the value used for the observed tide in the Gulf of Cadiz. We referred to this as the model unconstrained by the data. Model comparison and adjustment with the data are defined in terms of a minimization problem for a certain fitness function. This positive function grows as the estimates of the response depart from either observations or the prediction of the unconstrained model. If the observations consist only of sea surface height observations, as is the case here, the problem is poorly posed, a condition that can be further aggravated by poor observational sampling. This problem is remedied by defining a robust Tikhonov regularization scheme.

The results section includes a step-by-step analysis of the Mediterranean Sea response to distinct tidal forcing terms. The semi-enclosed basin normal modes are discussed and the synthesis of the tides in terms of these modes is carried out. These topics are treated using the unconstrained model. The regularized minimization problem is used to study the assimilation of tidal gauge data.

The major conclusions are set out in the final section.

MATERIALS AND METHODS

Tidal problem in the frequency domain

This section defines the model equations used to describe the barotropic response of a semi-enclosed sea to the gravitational attraction of the Moon and Sun for a given tidal constituent of frequency ω.

The body forces on the water include the direct effect due to the celestial gravitational potential Φ_0 and deviations from it induced by the deformable Earth. The latter contain two contributions, namely Φ_E due to the deformation of the Earth by the celestial gravitational body forces and Φ_L due to the deformation of the Earth by the load of the ocean tide. The total body force is $\vec{F} = -\nabla\Phi$ with $\Phi = \Phi_0 + \Phi_E + \Phi_L$.

In order to account for the tidally-induced deformation, the mean sea surface is defined as the long-time average of an equipotential surface (geoid plus oceanography). The tide η_g, considered positive upwards, is the sea surface deviation from this mean surface. The depth of the basin h is reckoned from the mean surface and is defined by a long time average of the bottom depth. The uplift with respect to this mean depth is given by $\eta_b = \eta_E + \eta_L$; where η_E, η_L are the contributions to the uplift due to the Earth and ocean tides, respectively.

In the following, the factor $e^{-i\omega t}$ is omitted and the velocity, surface heights and fluxes are complex valued. In the basin proper D the linearized equation of momentum is

$$-i\omega\vec{u} + \vec{\tau}_b / h + f\vec{k}\times\vec{u} + g\nabla\eta_g = -\nabla\Phi \qquad (1)$$

where $\vec{u}$ is the vertically-averaged horizontal velocity, h is the basin depth, f is the (variable) Coriolis parameter and g is the gravitational acceleration. A simple Rayleigh dissipation of the form $\vec{\tau} = C_d\, u^*\, \vec{u}$ is used to parameterize bottom friction, with constant drag coefficient C_d and typical bottom velocity u^*.

Using the fact that the Strait of Gibraltar width is small in comparison with a characteristic interior wavelength, the mass continuity equation is written in the form (Carrier *et al.*, 1971)

$$-i\omega(\eta_g - \eta_b) + \nabla.(h\vec{u}) - S\delta(\vec{x} - \vec{x}_1) = 0 \qquad (2)$$

where the last term is the flux per unit area exchanged with the strait. $\delta(\vec{x} - \vec{x}_1)$ is a Dirac delta function, $\vec{x}_1$ is the location of the mouth of the strait, and S is the flux across the strait.

The basin proper is otherwise assumed closed

$$h\vec{u}.\vec{n} = 0 \text{ in } \partial D_\alpha \alpha = 0,1,\ldots,I \qquad (3)$$

where $\vec{n}$ is the outward unit vector normal to the boundary and ∂D_α are the basin ($\alpha = 0$) and island ($\alpha = 1, \ldots, I$) boundaries. The boundary of the discrete model for the Mediterraean Sea in Figure 1 considers four islands, namely Majorca, Corsica-Sardinia, Crete and Cyprus.

With respect to a characteristic tidal wavelength the Strait of Gibraltar is narrow and relatively short. Under these conditions, changes of tidal transport along the strait are negligible and the momentum equation for the strait is given by the balance of pressure and the local acceleration. This assumption has been confirmed in the observations of Candela *et al.* (1990). Letting A_1, L_1, and r_1 be the mean values of the cross-section, the dynamic length and the friction coefficient $C_D\, u_1^* / h_1$ with u_1^* a typical bottom velocity and h_1 the mean depth of the strait, the momentum equation – at the strait – is simplified to

$$-i\omega A_1 u_1 + r_1 A_1 u_1 + \frac{A_1}{L_1}[g(\eta_g)_1 + (\Phi)_1 - g(\eta_g)_{o1} - (\Phi)_{o1}] = 0 \qquad (4)$$

Here the index o stands for the values at the ocean side of the strait. Mass flux and pressure continuity are required to be satisfied at the basin side of the strait.

$$S_1 = A_1 u_1, \eta_{g1} = \int_D \delta(\vec{x} - \vec{x}_1)\eta_g(\vec{x})d\vec{x} \qquad (5)$$

On the Atlantic side, the tide is assumed to be known from observation

$$\eta_{go1} = (\eta_g)_{ob} \qquad (6)$$

At island boundaries the circulation conditions

$$-i\omega\int_{\partial D}\vec{u}\cdot\vec{s}ds + \int_{\partial D_\alpha}\frac{1}{h}\vec{\tau}_b\cdot\vec{s}ds = 0;\quad \alpha = 1,\ldots,I \qquad (7)$$

are imposed in order to maintain pressure continuity in the multiply connected basin (Platzman, 1979).

Representation of forcing terms

The astronomical tidal potential and the deformation due to the Earth tide are both of large scale and are therefore well approximated in terms of spherical harmonics. Setting

$$\Phi_0 = -\sum_n U_n$$

where, U_n is the contribution of the n^{th} spherical harmonic. With this representation the effects of the Earth tide can be conveniently written using Love numbers (k_n and h_n), as an augmentation of the potential

$$\Phi_E = -\sum_n k_n U_n$$

and a deformation

$$\eta_E = \frac{1}{g}\sum_n h_n U_n$$

The sea surface tide is here defined by

$$\eta = \eta_g - \eta_b \qquad (8)$$

that is, η is the tide observed by tidal gauges and bottom pressure sensors. The excess pressure at the sea bottom $g\rho\eta$ causes both an augmentation of the potential and a deformation of the sea bottom. These effects can be written in terms of Love numbers (Hendershott, 1972; Accad and Pekeris, 1978); however, considering the smaller scales related to a semi-enclosed sea, a more appropriate representation is based on solving the response of the Earth to a surface point load (Farrell, 1972). In this approach the ocean tide load effects over a domain K are given by

$$\eta L(\vec{x}:K) = \int_K G_\eta(\vec{x},\vec{y})\eta(\vec{y})d\vec{y}$$

$$\Phi L(\vec{x}:K) = \int_K G_\Phi(\vec{x},\vec{y})d\vec{y}$$

The kernels $G_\eta(\vec{x},\vec{y})$ and $G_\Phi(\vec{x},\vec{y})$ represent the uplift and perturbation gravitational potential at $\vec{x}$ due to a delta function ocean tide at $\vec{y}$, and are obtained as solutions to an elasto-gravitational problem as formulated for instance by Alterman *et al.* (1959). The kernels are symmetric $G_\eta(\vec{x},\vec{y}) = G_\eta(\vec{y},\vec{x})$, $G_\Phi(\vec{x},\vec{y}) = G_\Phi(\vec{y},\vec{x})$ due to the reciprocity principle. In what follows a particular combination of these contributions enters into the hydrodynamic equations; thus defining

$$G(\vec{x},\vec{y}) = G_\eta(\vec{x},\vec{y}) - \frac{1}{g}G_\Phi(\vec{x},\vec{y}) \qquad (9)$$

the total effect of the ocean tidal load in the domain K is given by

$$\eta_T(\vec{x}:K) = \int_K G(\vec{x},\vec{y})\eta(\vec{y})d\vec{y} \qquad (10)$$

Available estimates of the kernels use spherical symmetric earth models. For this class of models $G(\vec{x},\vec{y}) = G(s)$; $s = |\vec{x}-\vec{y}| = r_e\delta$ where $r_e = 6.371\ 10^6$ (m) is the mean radius of the Earth and δ is the angle subtended by $\vec{x}$ and $\vec{y}$ at the centre of the Earth. In this work the kernels computed by Francis and Mazzega (1990) from the Preliminary Reference Earth Model are used. In the computation of $\eta_T(\vec{x}:D)$ for $\vec{x}$ in D, the transfer functions are given by

$$G_\eta = \rho_w F_\eta(\theta)\ ;\quad G_\Phi = \rho_w F_\Phi(\theta)$$

$$G = G_\eta - 1/g\, G_\Phi$$

and the F's are the transfer functions tabulated in Francis and Mazzega (1990) using Farrell's (1972) notation, $F_i = f_i/(10^{12} r_e \theta_i)$, with $r_e = 6.371\ 10^6$.

In order to introduce the tidal load contributions, the semi-enclosed basin domain is separated into the basin proper D and the Strait of Gibraltar with domain D_1. The portion of the World Oceans outside the semi-enclosed basin is denoted by O. The momentum equation 1, using (9-10), replacing η_g with the ocean tide η, takes the form

$$-i\omega\vec{u} + \vec{\tau}_b/h + f\vec{k}\times\vec{u} + g\nabla(\eta + \eta_T(\vec{x}:D))$$
$$= \nabla(\sum_n U_n(1+k_n-h_n)) + g\nabla(\eta_T(\vec{x}:O) + \eta_T(\vec{x}:D_1))$$

As noted in the Introduction, these are integro-differential equations. For the sake of completeness the momentum equation in the Strait is given by

$$\begin{aligned}
&-i\omega A_1 u_1 + r_1 A_1 u_1 \\
&+\frac{A_1}{L_1}[g(\eta)_1 - (\sum_n U_n(1+k_n-h_n))_1 + g\eta_T((\vec{x}_1:D) \\
&+g\eta_T(\vec{x}_1:O) + \eta_T(\vec{x}_1:D_1) \\
&-g(\eta)_{o1} + (\sum_n U_n(1+k_n-h_n))_{o1} \\
&-g\eta_T(\vec{x}_{o1}:D) - g\eta_T(\vec{x}_{o1}:O) \\
&\eta_T(\vec{x}_{o1}:D_1)] = 0
\end{aligned} \qquad (11)$$

Application to the M_2 tide

The equilibrium tide, the Love numbers, and the frequency of the M_2 tide are approximated by

$$\begin{aligned}
&\eta_{eq} = 0.2425 \sin^2\theta e^{-2i\lambda}(1+k_2-h_2)\ (m) \\
&k_2 = 0.3024,\ h_2 = 0.6126 \\
&\omega = 1.405\ 10^{-4}\ rad/s
\end{aligned} \qquad (12)$$

where θ and λ are the co-latitude and longitude respectively.

The contribution of the local tidal load term η_L, in a limited area basin, can be roughly estimated by the ratio of the uplift η_L to a tidal load η with a horizontal scale l_0. Under these conditions η_L/η grows linearly with l_0/r_e and for a tidal signal with a scale of about 1000 km (possibly the largest scale signal in the Mediterranean), the expected maximum depression will be in the order of 3 % of η.

Estimates of the forcing terms in the strait show that they are negligible except for the bottom friction term. There-

fore, with these simplifications, the system of equations used in the study of the M_2 tide are:

$$-i\omega\vec{u} + \vec{\tau}_b / h + f\vec{k}\times\vec{u} + g\nabla[\eta + \eta_T(\vec{x},D)] = g\nabla(\eta_{eq}) + g\nabla[\eta_T(\vec{x}:O)] \quad (13)$$

$$-i\omega\eta + \nabla.(h\vec{u}) - S\delta(\vec{x} - \vec{x}_l) = 0 \quad (14)$$

$$-i\omega A_l u_l + rA_l u_l + \frac{A_l}{L_l}[g\eta_l - g\eta_0] = 0 \quad (15)$$

$$S = A_l u_l,\ \eta_l = \int_D \delta(\vec{x} - \vec{x}_l)\eta(\vec{x})d\vec{x} \quad (16)$$

and the circulation conditions (7).

In order to limit the influence of observations in the tuning of the physical parameters of the model, the bottom friction parameter used in the Strait of Gibraltar is $r_e = 4.83\ 10^{-5}$ (1/s) following Candela (1991). In the interior of the basin, the value of $C_D\ u^* = 2\ 10^{-4}$ (m/s) was used for bottom dissipation. It was found that the results were quite insensitive to modification of the interior dissipation within a factor of two.

The tuning of the model was limited to small changes to the geometrical parameters describing the Strait of Gibraltar and of the observed tide in the Atlantic Ocean side of the strait. The selected values are:

$$\left.\begin{array}{l} A_l = 7.3\ 10^6\ m^2;\ L_l = 60\ km;\ |\eta_0| = 0.78; \\ \text{phase}\ (\eta_0) = 56^o \end{array}\right\} \quad (17)$$

Spectral representation

Following and extending Proudman (1938) to include straits and islands, a spectral representation of the system of equations (7), (13-16) as defined in Candela and Lozano (1994) is used. Here we complement the outline given in the Introduction, and the reader is referred to the above-mentioned source for further details.

The vertically-averaged horizontal velocity in terms of the Helmholtz-Proudman potentials is

$$\vec{u} = \nabla\phi + \frac{1}{h}\vec{k}\times\nabla\psi \quad (18)$$

In this representation the divergence of the transport $h\vec{u}$ is given by $\nabla\cdot h\nabla\phi$ and the relative vorticity of the vertically averaged velocity is $\nabla\cdot h^{-1}\nabla\psi$.

The Helmholtz-Proudman potentials ϕ, ψ are expanded in terms of the eigenfunctions of the elliptic boundary problems:

$$\nabla.(h\nabla\phi_i) = -\lambda_i\phi_i;\ h\nabla\phi_i.\vec{n} = 0 \text{ at } \partial D_\alpha,\ \alpha = 0,...,I \quad (19)$$

$$\nabla.(h^{-1}\nabla\psi_i) = -\mu_i\psi_i;\ \psi_i = 0 \text{ at } \partial D_\alpha,\ \alpha = 0,...,I \quad (20)$$

The boundary conditions reflect the fact that each velocity component separately satisfies the kinematic condition of no-flow across the outer boundary of the basin and at each island.

For each island an auxiliary function $\psi_{(\alpha)}$ is defined by

$$\nabla\cdot\left(h^{-1}\nabla\psi_{(\alpha)}\right) = 0;\ \psi_{(\alpha)} = \delta_{\alpha\beta} \text{ at } \partial D_\beta,\quad \alpha,\beta = 1,...,I;$$
$$\psi_{(\alpha)} = 0 \text{ at } \partial D_0 \quad (21)$$

The velocity potentials can be approximated uniformly by the series

$$\phi = \sum_{i=1}^{J} P_i(t)\phi_i(\vec{x})$$
$$\psi = \sum_{i=1}^{L} Q_i(t)\psi_i(\vec{x}) + \sum_{\alpha=1}^{I} Q_{(\alpha)}(t)\psi_{(\alpha)}(\vec{x}) \quad (22)$$

The surface height is approximated non-uniformly by the series

$$\eta = \sum_{i=0}^{J} N_i(t)\eta_i(\vec{x});\ \eta_i = c_i\phi_i \quad (23)$$

and the c_i are suitable scaling constants.

Projecting the model equations (13-16) on to the basis functions (19-21) leads to a system of algebraic equations. In the present context the essential properties of the algebraic equations are expressed in matrix notation as follows:

$$-i\omega\,\mathbf{U}\mathbf{y} + \mathbf{M}\mathbf{y} = \mathbf{f} \quad (24)$$

for the state vector $\mathbf{y} = \begin{pmatrix} N \\ P \\ Q^{ext} \\ S \end{pmatrix}$

where the N, P are column vectors formed with the coefficients of η, and ϕ, respectively,

$$Q^{ext} = \begin{pmatrix} Q \\ Q_\alpha \end{pmatrix}$$

is a column vector formed with the coefficients of the eigenfunctions ψ and the auxiliary functions $\psi_{(\alpha)}$ and S is the flux across the Strait of Gibraltar.

The structure of the matrices **U**, **M**, and **f**, partitioned in blocks as the vector **y** are now summarized. **U** is a symmetric block diagonal matrix with identity matrices in all the blocks in the diagonal except the block associated to Q_α. In this case the block in the diagonal is a symmetric positive definite matrix associated to the circulations around islands. The matrix **M** is split into

$$M = M_s + M_a \quad (25)$$

where the symmetric part $\mathbf{M_s} = \mathbf{D_s} + \mathbf{T_s}$ consists of

$$D_s = \begin{bmatrix} Z & Z & Z & Z \\ Z & [0,0] & \{0,-1\} & Z \\ Z & -\{0,-1\}' & [0,-2] & Z \\ Z & Z & Z & r \end{bmatrix}$$

which contains bottom friction contributions, and of

$$T_s = \begin{bmatrix} Z & \frac{1}{2}vG & Z & Z \\ \frac{1}{2}G'v' & Z & Z & Z \\ Z & Z & Z & Z \\ Z & Z & Z & Z \end{bmatrix}$$

containing the symmetric part of the local ocean tidal load effects. Here Z denotes null matrices of the appropriate sizes, and the transpose of a matrix A is denoted by A'. The antisymmetric contribution $\mathbf{M}_a = \Omega_a + T_a$ includes the Coriolis (gyroscopic) effects

$$\Omega_a = \begin{bmatrix} Z & -v & Z & -[v] \\ v' & \{1,1\} & [1,0] & Z \\ Z & -[1,0]' & \{1,-1\} & Z \\ [v]' & Z & Z & Z \end{bmatrix}$$

and the local ocean tidal load effects

$$T_a = \begin{bmatrix} Z & \frac{1}{2}vG & Z & Z \\ \frac{1}{2}G'v' & Z & Z & Z \\ Z & Z & Z & Z \\ Z & Z & Z & Z \end{bmatrix}$$

The frequency matrix is $v = \mathrm{diag}\,(v_0, v_1, \ldots)$, where v_i are the frequencies of the closed non-rotating basin normal modes, and **G** contains the contributions from the local tidal load terms. The entries of the blocks denoted with the symbols [p,q], {p,q} are symmetric and anti-symmetric matrices, respectively. The entries of these matrices are integrals containing weights of the form $f^p h^q$. These blocks in the anti-symmetric matrix Ω_a are due to the vorticity stretching terms.

The forcing vector has the equilibrium tide contribution N_e, the Atlantic forcing tide N_A, and the World Ocean tidal load P_0,

$$\mathbf{f} = \begin{pmatrix} vN_e \\ P_0 \\ 0 \\ [v]\mathbb{N}_A \end{pmatrix} \qquad (26)$$

The Helmholtz-Proudman basis functions are constructed using a finite difference scheme to solve the eigenvalue problems (19), (20), and the boundary problem (21) over a grid with uniform spacing (nominal 20 km) and with the discrete boundary shown in Figure 1. The number of degrees of freedom is approximately 17 000, and a satisfactory resolution of the gravitational modes is obtained using J = 100 ϕ s, L = 250 ψ s, I = $4\psi_{(\alpha)}$ s and one strait. Thus the state vector **y** has exactly 454 components.

Normal modes

A thorough review of basin normal modes can be found in Platzman (1978). Here a brief outline of relevant results is given. The (right Y_r / left Y_l) eigenvectors are defined by the solutions to

$$\left(-i\omega_r \mathbf{I} + \mathbf{U}^{\frac{1}{2}}\mathbf{M}\mathbf{U}^{\frac{1}{2}}\right)\mathbf{Y}_r = 0$$

$$\mathbf{Y}_l\left(i\omega_l + \mathbf{U}^{\frac{1}{2}}\mathbf{M}\mathbf{U}^{\frac{1}{2}}\right) = 0$$

respectively. For each eigenfrequency associated with a right eigenvector there is a left eigenvector associated with its complex conjugate. Omitting the symmetric part $\mathbf{D}_s + \mathbf{T}_s$ of **M**, the eigenfrequencies are real and left and right eigenvectors coincide. The Rayleigh dissipation represented by the matrix $\mathbf{D}_s$ is, by design, positive definite (dissipative). The symmetric part of the local tidal load $\mathbf{T}_s$ requires some consideration. It transpires that this matrix is as well positive definite, and this is due to two facts: (1) The kernels (9) are symmetric, due to the reciprocity principle, for the elasto-gravitational problem; and (2) the kernels have a unique sign over the domain. For larger domains the kernels change sign due to the buckling of the Earth, and the second condition does not necessarily hold.

The forced response of a basin can have a structure quite different from any of the normal modes that its geometry can support. However, if either the spatial structure of the forcing or its time periodicity matches one or several of the normal modes, it is reasonable to expect a resonant response that will relate to the excitation of these modes. For the semidiurnal tides in the Mediterranean Sea this is particularly the case because of several modes that closely match either the spatial structure or the periodicity of the forcing functions, whether of the independent tide or of the co-oscillating tide with the North Atlantic. This information is implicitly contained in the coefficients (a_n) resulting from the projection of the tidal forcing onto the set of normal modes resolved. These coefficients are given by

$$a_n = \frac{i}{\omega - \omega_n}\frac{\mathbf{Y}_{ln}^{\mathbb{C}}\mathbf{U}^{\frac{1}{2}}\mathbf{f}}{\mathbf{Y}_{ln}^{\mathbb{C}}\mathbf{Y}_{rn}} \qquad (27)$$

where $\mathbf{y} = \sum_n a_n \mathbf{Y}_{rn}$ is the solution to (24). A closer examination of these coefficients is taken up in the section entitled "Results".

Energy balance and energy exchanges

The average potential energy $\overline{pe}$ and kinetic energy $\overline{ke}$ associated with the semi-enclosed sea are given by

$$\overline{pe} = \frac{1}{2}\mathbf{N}\mathbb{C}\mathbf{N},\ \overline{ke} = \frac{1}{2}\mathbf{P}\mathbb{C}\mathbf{P} + \frac{1}{2}\mathbf{Q}^{ext}\mathbb{E}^{ext}\mathbf{Q}^{ext} + \frac{1}{2}\mathbf{S}\mathbb{C}\mathbf{S} \qquad (28)$$

and the total energy $\bar{e} = \overline{pe} + \overline{ke} = \frac{1}{2}\,\mathbf{y'Uy}$. After multiplying (24) by $\mathbf{y'}$, it follows that the power $-i\omega\,\bar{e}$ of the system satisfies

$$-i\omega\bar{e} + \mathbf{y'}\,D_s\,\mathbf{y} + \mathbf{y'}T_s\,\mathbf{y} = \mathbf{y'f} \tag{29}$$

The righthand-side is the work done to the system by the combined gravitational forces, the Atlantic tidal forcing and the tidal load of the world oceans.

The antisymmetric part of the system does not contribute directly to the energy balance but redistributes the energy within the system. The bilinear forms $-N'vP$, $-N'[v]S$ and $-\frac{1}{2}N'vGP$ are the contributions to the energy exchanged from $\overline{pe}$ to the basin irrotational kinetic energy. The planetary and topographic beta effects yield the term $P'[1,0]Q^{ext}$ representing exchanges from irrotational to rotational kinetic energy; and the term $P_i\{1,1\}_{ij}\,P_j$ and $Q_i\{1,-1\}_{ij}\,Q_j$ are responsible for energy exchanges between irrotational and rotational modes, respectively.

Comparison with observations and the melding of model and data

In this section a method to meld the data and the model is introduced. The motivation is to combine both data and model information in the estimate of the state vector **y**, maintaining to the greatest extent possible a distinction between the dynamical information of the model and the information of the data in the dynamics. In this way, further improvement in the understanding of the dynamics is facilitated.

We start by introducing some definitions. The sea surface height amplitude η defined in (23) can be seen as an interpolator in terms of a finite set the Proudman basis functions η_j, j = 1, ..., J. Given a set of observation points $\bar{x}_k$, k = 1, ..., k the matrix $\mathbf{C}_I$ defined by $\mathbf{C}_{Ikj} = \eta_j(\bar{x}_k)$, maps the coefficient vector $N = [N_1, ..., N_j]$, to the amplitude vector $\eta = \mathbf{C}_I N$. The extended matrix $\mathbf{C} = [\mathbf{C}_I Z]$, where Z is an appropriate null matrix permits us to write the last equation in the form

$$\eta = \mathbf{C}y \tag{30}$$

For a given state vector **y**, and observation vector η_{ob} where $\eta_{ob\,k} = \eta_{ob}(\bar{x}_k)$, k = 1, ..., K, the data residual vector is defined by

$$\mathbf{d} = \eta_{ob} - \mathbf{C}y$$

and, for a given state vector **y**, the model residual is defined by

$$\mathbf{r} = -i\omega\,\mathbf{U}y + \mathbf{M}y - \mathbf{f}$$

The model estimate $\mathbf{y}_M$ is obtained by setting the model residual **r** to zero; that is by the solution of (24). The data residual associated with the model estimate is $d_M = \eta_{ob} - Cy_M$. In terms of the departure from the model solution, the data and model residuals are

$$d = d_M - Cs \tag{31}$$

$$r = -i\omega\,Ys + Ms \tag{32}$$

respectively. The model estimate $\mathbf{y}_M$ does not use information from the set of observations, and the data residual $\mathbf{d}_M$ measures the misfit between the data and the model. In order to meld the data and the dynamic information contained in the model a fitness function, depending upon a non-negative parameter γ, is defined by

$$F(s,\gamma) = \gamma\,r'r + d'd \tag{33}$$

In this section prime stands for the transpose conjugate operator. The fitness function is a positive quadratic function of **s** and for each γ it has a minimizer s_γ, that is $F(s_\gamma,\gamma) \le F(s,\gamma)$, for all s. For $\gamma = 0$, the model is ignored and the approximation is the best fit among the functions defined by (23) to the observations. At the other extreme, for $\gamma = \infty$, s = 0, the data is ignored, and the model estimate $\mathbf{y}_M$ is recovered.

For a given $\gamma > 0$, the minimum $F(\gamma) = F(s_\gamma,\gamma)$ and the minimizer s_γ of F are obtained after substitution of (31), (32) in (33) and completing the squares. Let

$$B = [-i\omega\,\mathbf{U} + \mathbf{M}]'\,[-i\omega\,\mathbf{U} + \mathbf{M}]$$

The hermitian and invertible matrix **B** is written in the form $\mathbf{B} = \mathbf{Q}\Lambda\mathbf{Q}'$; where $\Lambda = \mathrm{diag}(\lambda_1, ..., \lambda_m)$ are the eigenvalues of **B**, the columns of **Q** are its corresponding eigenvectors and m is the dimension of the state vector **y**. Define now

$$C = C\left(\Lambda^{\frac{1}{2}}Q\right)^{-1} \tag{34}$$

then

$$F(\gamma) = d'_M d_M - d'_M C[\gamma\,E + C'C]^{-1}C'd_M \tag{35}$$

$$s_\gamma = \left[\Lambda^{\frac{1}{2}}Q\right]^{-1}[\gamma\,E + C\,C]^{-1}C\,d_M \tag{36}$$

where E is the identity matrix.

In order to examine the properties of the solution, and at the same time provide a robust computational algorithm, we introduce the singular value decomposition of C defined by its singular (positive) values μ_n and the orthonormal vectors e_n z_n such that

$$Cz_n = \mu_n e_n\,;\; C'e_n = \mu_n z_n$$

Using now the expansion $d_M = \sum_n e_n\,d_M\,e_n + d_M$, where $C\,d_M = 0$, the minimum and the minimizer can now be written in the form

$$F(\gamma) = d_M\,d_M - \sum_n \frac{\mu_n^2\,|e_n\,d_M|^2}{\gamma + \mu_n^2} \tag{37}$$

$$s_\gamma = \sum_n \frac{\mu_n e_n\,d_M}{\gamma + \mu_n^2}\left[\Lambda^{\frac{1}{2}}Q\right]^{-1} z_n \tag{38}$$

Consider again the case $\gamma = 0$. The minimum $F(0) = \tilde{d}_M' \tilde{d}_M$ is the magnitude square of the component $\tilde{d}_M$ of d_M lying in the null space of C'. The vector $\tilde{d}_M$ represents that part of the observations that is not observable by the dynamic system. The minimizer s_0 cannot be computed safely since small deviations in d_M will introduce errors of order μ_n^{-1}.

A stable solution of (37) is obtained by considering the constrained minimization problem (Tikhonov and Arzenin, 1977): For a given positive number δ, determine $\gamma(\delta)$ such that $F(\gamma(\delta)) \leq F(\gamma)$, for $\gamma > 0$ and $s_\gamma' s_\gamma \leq \delta^2$. In practice, δ is taken as a given fraction a of the magnitude of model solution y_M and, in fact, we consider only the case

$$\delta = \alpha [y_M' y_M]^{\frac{1}{2}} \tag{39}$$

RESULTS

The response of the Mediterranean Sea to distinct tidal forcings

In this section the response of the Mediterranean Sea to the different tidal forcings is described by introducing them one at a time, in order to quantify their individual contributions to the observed total response. The symbols referred to below are defined in (24)-(26) above.

Co-oscillation: $N_A \neq 0$, $Ne \neq 0$, $P_O = 0$, $G = 0$. First we disregard the astronomical tidal potential acting over the basin and consider only the forcing through the Strait of Gibraltar, *i.e.* that in equation (24) due to the tide in the Atlantic Ocean. Figure 2*a* shows, as may be expected, that the largest amplitudes are found at the mouth of the strait, followed by appreciable values in the Gulf of Gabes and the north of the Aegean Sea. The phase (Fig. 2*b*) indicates the presence of an amphidromic point south of the island of Ibiza in the Western Mediterranean, another in the Adriatic Sea and yet another around the western end of Crete. Later on, when analysing the energy budget of the basins, we shall see that this co-oscillating tide with the Atlantic represents the largest net tidal input into the system.

Independent tide: $N_A \neq 0$, $N_e \neq 0$; $k_2 = h_2 = 0$; $P_O = 0$, $G = 0$. The effect due to the direct forcing of the tidal potential over the Sea is introduced keeping the strait "open", in the sense that flows can exist there in response to the pressure gradient set by sea-level changes inside the Sea with a constant (zero value) mean sea level outside. This independent tidal forcing shows (Fig. 2*c*) a response that is concentrated in the Eastern Mediterranean basin, with associated large amplitudes in the Gulf of Gabes as well as at the head of the Adriatic Sea and the head of the Aegean Sea near the mouth of the Dardanelles Strait. The amplitudes inside the Western Mediterranean basin are less than 5 cm. There is also an amphidromic point in the Adriatic, however, its phase pattern (Fig. 2*d*) is 180° apart from that present by the co-oscillating tide discussed earlier. This 180° phase difference can also be observed throughout the eastern basin, therefore, the co-oscillating and independent tides oppose each other in most of the Eastern Mediterranean basin. The independent tide presents nodal lines (degenerated amphidromic points) in the Strait of Sicily and north and south of the western tip of Crete.

Combined tides: $N_A \neq 0$, $N_e \neq 0$; $k_2 = h_2 = 0$; $P_O = 0$, $G = 0$. The superposition of the co-oscillating and independent tides leads to a pattern (Fig. 3*a* and 3*b*) with well-defined amphidromic points in the Adriatic Sea and the Strait of Sicily, and nodal lines running meridionally south and north of the western side of Crete. In the Western basin there is a degenerated amphidromic point south of Valencia, Spain. The largest amplitudes are observed at the head of the Adriatic Sea and in the Gulf of Gabes, with appreciable amplitudes also in the Alboran and Aegean Seas. This co-tidal pattern would be close to the real tide if the Earth was a rigid solid; however, this is not the case and account most be taken of the fact that the Earth also yields appreciably to the tidal forces and therefore contributes to the observed response.

Combined tides and Earth tide: $N_A \neq O$, $N_e \neq 0$; $k_2 \neq 0$, $h_2 \neq 0$, $P_O = 0$, $G = 0$. The effect the Earth tide has on the Sea's tidal response can be seen in Figures 3*c* and 3*d*. Comparing these patterns with those of Figures 3*a* and 3*b*, it can be seen that the contribution of the Earth tide implies an appreciable reduction (~30%) in the amplitude of the tide in the Sea, which is particularly evident in the Eastern Mediterranean.

The deformable Earth not only yields to the astronomical tidal forces, but also deforms under surface loads due to the varying thickness of the water column. The tidal load effects in a semi-enclosed sea are conveniently separated into those due to the Global Ocean tide and those due to the Sea local tide. As mentioned earlier, the magnitude of the deformation depends on the horizontal scale of the applied load, therefore, it is expected that the Global Ocean tide will have a larger contribution to the Mediterranean bottom deformation, even though it represents a non-local load effect. Figures 4*a* and 4*b* show the deformation of the bottom of the Mediterranean Sea due to the observed M_2 tide on the world's oceans using in equation (10) the tide estimate of Cartwright and Ray (1990) deduced from satellite altimetry. The response to this effect is of large scale with maximum amplitude of 1.2 cm in the Alboran Sea and decreasing towards the Eastern Mediterranean. The phase of this deformation is nearly constant throughout the whole domain with a value of 270°. The deformation due to the local tide (Fig. 4*c* and 4*d*), of smaller spatial scale, has a magnitude in the order of a few millimetres.

All forcings included: Combining now all the forcing terms, the M_2 tide sea surface elevation and transports are shown in Figures 5 and 6. The maximum tidal transports are observed in the Alboran Sea and to a lesser degree in the Algerian basin and south of Crete in the Eastern Mediterranean. Tidal currents tend to be nearly rectilinear in most of the Sea with a marked exception in the area to the north of Tunisia, between Sardinia and Sicily, where tidal currents show a pronounced ellipticity. The presentation of transports is somewhat deceptive in that they are weighted by depth; a similar plot showing the tidal barotropic currents (not shown) indicates that the largest tidal currents occur in the northern part of the Adriatic Sea, the Gulf of Gabes, the Sicilian Channel, the Alboran Sea and in some parts of the Aegean, in order of decreasing magnitude. Figure 6*b* shows contours of the phase of the tidal flows corresponding to the time when the tidal transport is maximum,

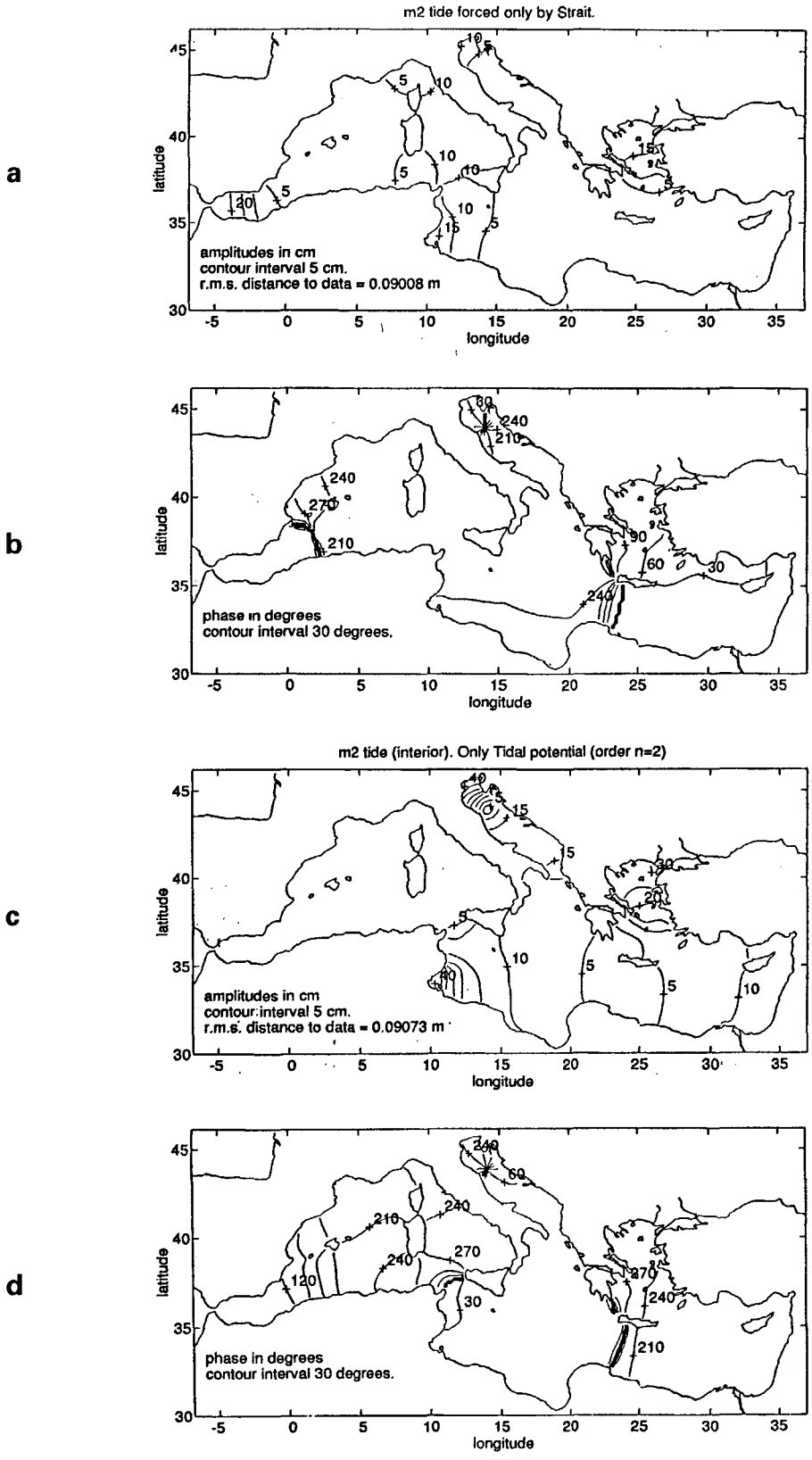

Figure 2

Co-oscillating and independent tide response of the Mediterranean Sea. (a) Sea surface elevation amplitude obtained when considering only the co-oscillating tide from the North Atlantic entering through the Strait of Gibraltar. Contours of amplitude in centimetres with a contour interval of 5 cm. The rms error with respect to the 60 observed tide gauge stations is also indicated. (b) Co-oscillating tide cophase lines in degrees with respect to the Greenwich meridian with a contour interval of 30°. (c) Sea surface elevation amplitude obtained when considering only the astronomical tidal potential acting over the Mediterranean basin. The Strait of Gibraltar is maintained open but a constant sea level is considered outside. (d) Independent tide cotidal lines in degrees (GMT).

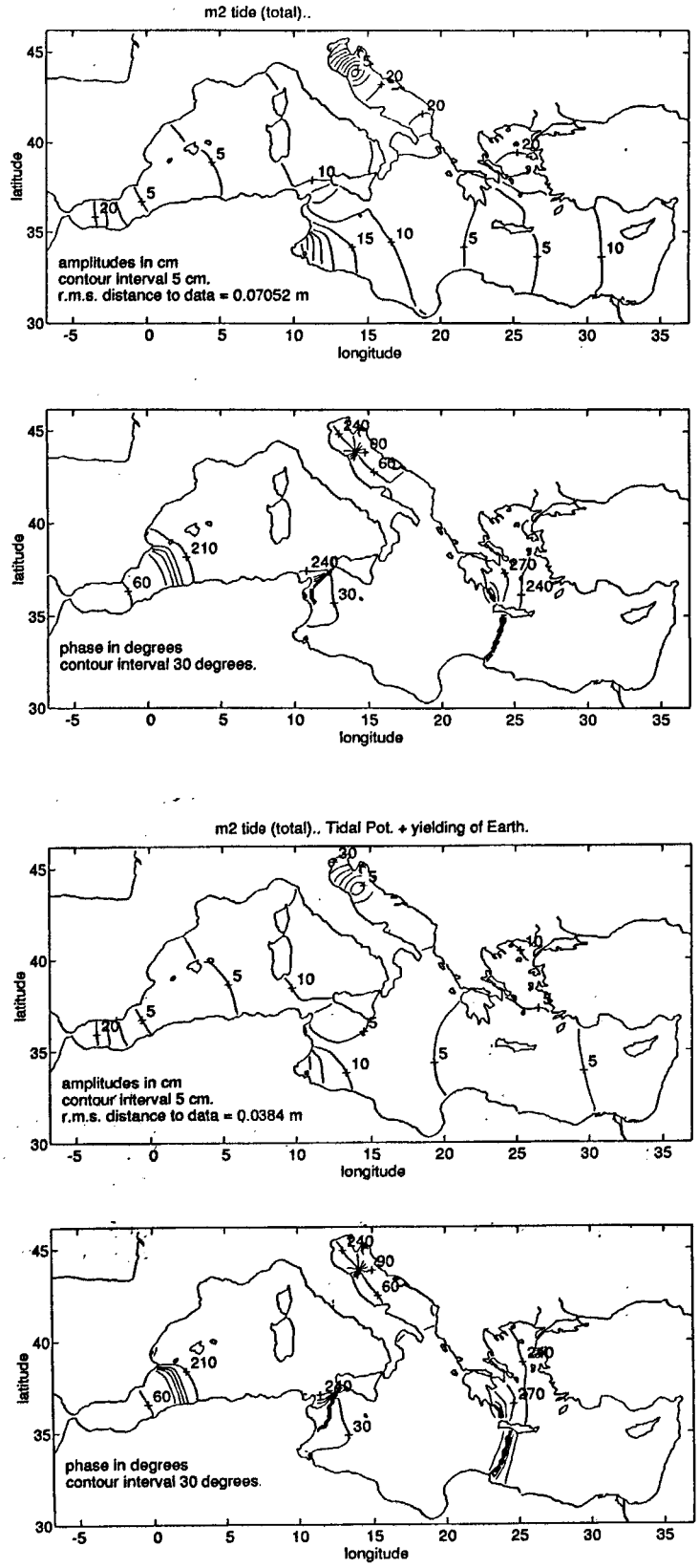

Figure 3

Sea-surface elevation amplitude (a) and phase (b) obtained when considering both the co-oscillating North Atlantic tide and the direct tide forced by the astronomical tidal potential. Sea surface tidal response [amplitude (c) and phase (d)] of the tide in (a) and (b) corrected for the effect of the Earth's tide.

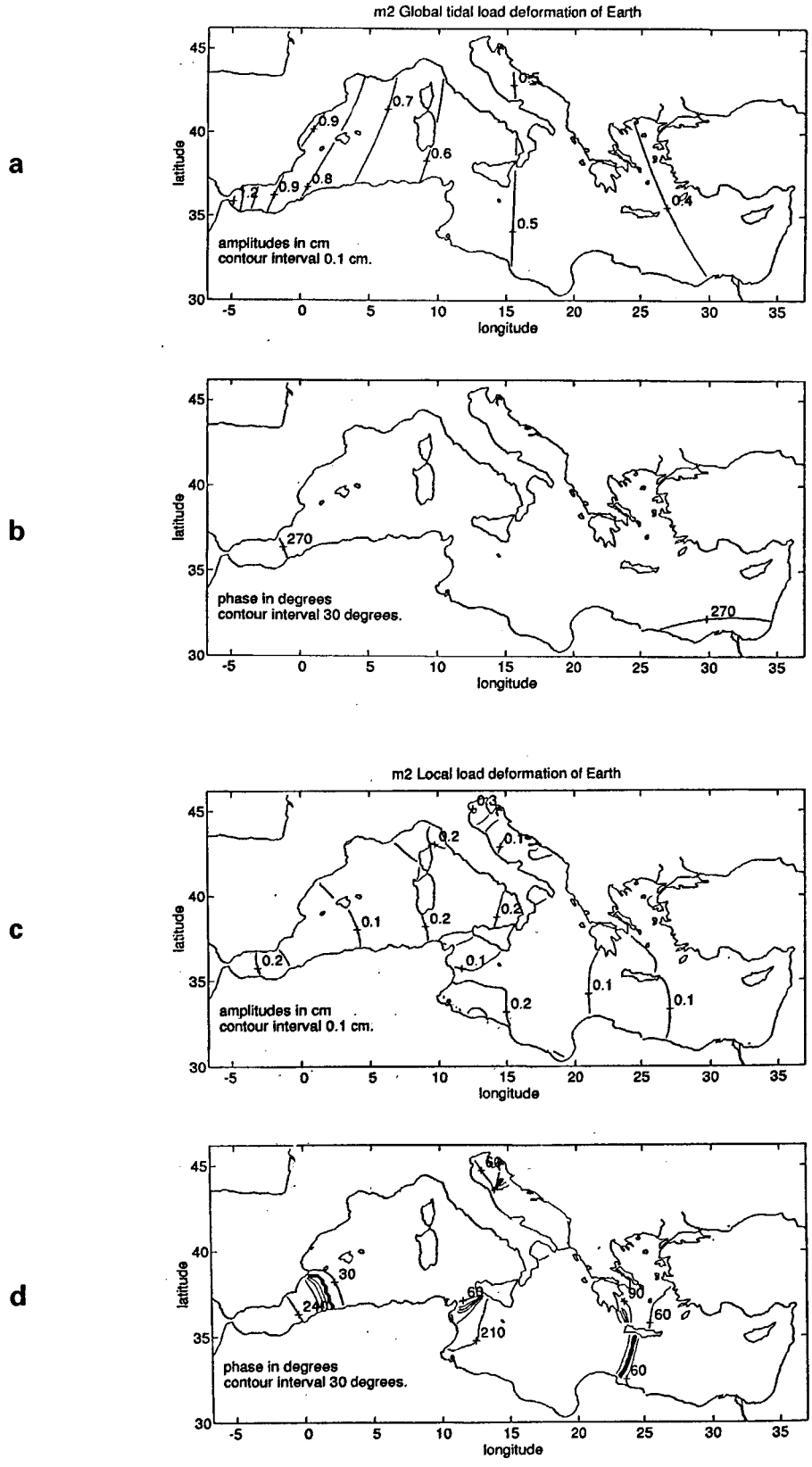

Figure 4

Deformation of the bottom of the Mediterranean Sea due to the load effect of the World Ocean tide computed with the observed cotidal charts deduced from two years of GEOSAT altimetric data (Cartwright and Ray, 1990) and the deformation kernels of Francis and Mazzega (1990). (a) Constant amplitude lines in centimetres and (b) constant phase lines in degrees (GMT). Deformation of the bottom of the Mediterranean Sea due to the local tidal load effect. (c) Constant amplitude lines in centimetres and (d) constant phase lines in degrees (GMT).

Figure 5

Sea surface tidal response of Figures 3c and d corrected by the effect of the deformation of the bottom of the Mediterranean Sea due to the global and local tidal load effects. Upper panel co-range lines in centimetres and lower panel cotidal lines in degrees (GMT).

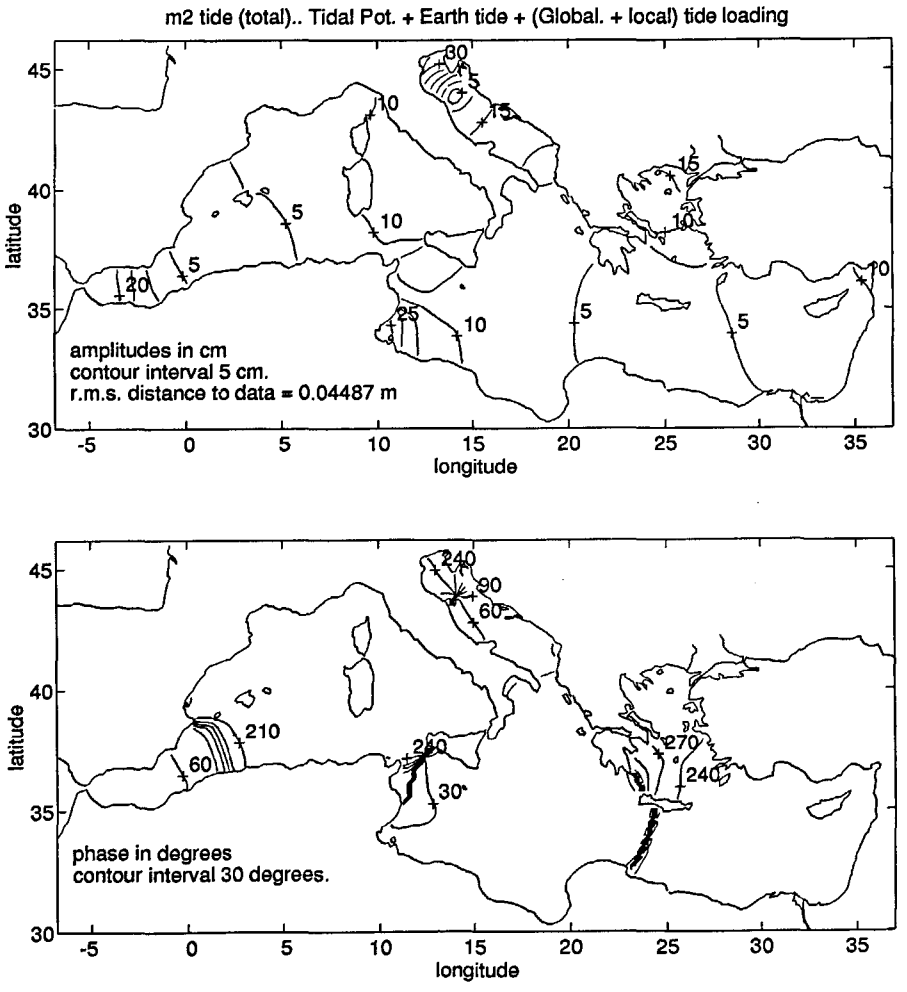

i.e. oriented along the semi-major axis of the tidal current ellipse. It is difficult unambiguously to construct phase contours of tidal flows over a large area. Here we have chosen to show the phase when the transport semi-major axis falls in the first or fourth trigonometric quadrants, that is to the right of the north-south line. The phase of the tidal flows seems to be quite constant throughout the whole Sea and very similar to that corresponding to the flooding tide at Gibraltar, *i.e.* 130°. The region south of Sicily which has a nearly constant phase of 300° is indicative of westward tidal flows there at the time when the surrounding regions have currents flowing in an eastward direction. There is the presence of a tidal current amphidromic point in the southern part of the Adriatic Sea associated with the sea surface system observed there (Fig. 5*b*), although our rough discretization is not able to reproduce it in all its detail. Also at some points along the Mediterranean coast there are rapid phase changes near embayments and in places with appreciable depth relief. In general, these modelled tidal currents reproduced very closely the tidal current ellipse parameters for the few places in the Western Mediterranean where available observations have permitted the extraction of the M_2 current tidal harmonics (see Albérola *et al.*, 1995).

The interaction of the Atlantic co-oscillating tide and the independent tide in determining the observed Mediterranean M_2 tide can be seen in the tidal transports shown in Figures 6*c* and 6*d* at the time of maximum flood at the Strait of Gibraltar and a quarter of a cycle later. The tidal flows through Gibraltar set the tidal rhythm in the Sea.

Tidal energy flux, energy flux divergence and net energy balance

Given the available model results for the sea surface elevation (Fig. 5) and transport (Fig. 6) patterns, the net tidal energy flux vectors, shown in the upper panel of Figure 7, are computed by (Godin, 1988): $\mathbf{P} = 1/2\ \rho\ rgh\ [M \cos\theta, -m \sin\theta]$, where: ρ is mean water density, g is acceleration due to gravity, η is the tidal constituent sea surface elevation amplitude, M is the semi-major axis of the current ellipse, m the semi-minor axis and θ the phase difference between high water and maximum tidal current. The net tidal energy flux entering through the Strait of Gibraltar is approximately 6.5 10^8 W. There are net energy transfers into the Eastern Mediterranean through the Strait of Sicily and into the Adriatic Sea through the Strait of Otranto. There is also some net tidal energy leaving the Aegean Sea into the Ionian, between the island of Crete and mainland Greece. A complementary quantity is the divergence of the energy flux vector shown in Figure 7 (lower panel). The units of the energy flux divergence are in W/m and positive values are indicative of areas where there is a loss of tidal energy, for example in the Alboran Sea, where a large part of the losses are taking place, and also in some parts of the

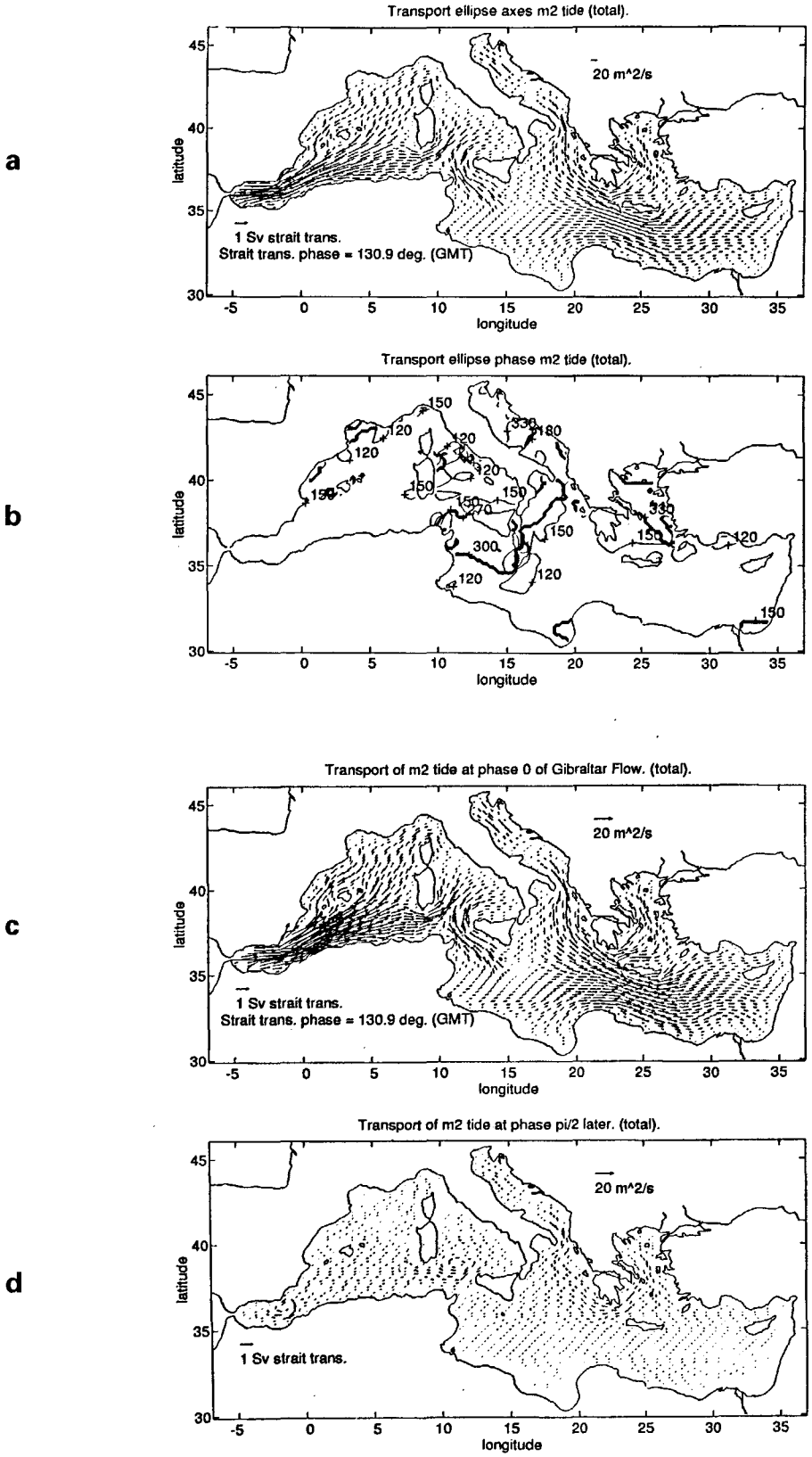

Figure 6

Tidal transport ellipses associated with the sea surface elevation patterns shown in Figure 5. (a) Tidal ellipse axes in m^2/s with the scale indicated in the upper part of the Figure. The transport amplitude through the Strait of Gibraltar is given in Sverdrups (1 Sverdrup = 10^6 m^3/s), with the scale indicated. (b) Contours of constant tidal transport phase in degrees with respect to Greenwich. (c) Instantaneous tidal transports at the time of maximum flooding tide through the Strait of Gibraltar and a quarter of a cycle later (d). The scale of the transport vectors is indicated in the upper right hand corner of each panel.

Aegean, the Adriatic, the Strait of Sicily and the Tyrrhenian. Negative values of the energy flux divergence are indicative of tidal energy convergence. These are places where the tide is doing net work on the Sea circulation.

The power balance for the entire basin is obtained by evaluating the terms in the power equation (29). The righthand term in the equation contains the power input into the system, which consists of the net energy flux entering through the Strait of Gibraltar (6.52 10^8 W) and the work done by the astronomical tidal potential over the Sea (–4.89 10^8 W). This latter quantity is already taking into account the ~30% reduction due to the energy extracted by the Earth tide from the system. As mentioned previously, the distributions seen in Figure 2 indicate that the tidal potential does work in opposition to that done by the tide entering through Gibraltar, resulting in a net tidal power input into the system of only 1.63 10^8 W. This power gets dissipated by bottom frictional stresses (–0.94 10^8 W), the second term in the left hand side of equation 29 and by transmission into the lithosphere by the bottom deformation due to the global tidal load (–0.62 10^8 W) included in the right hand term, and the local tidal load (–0.07 10^8 W) included in the third term in the lefthand-side of the power equation. These calculations show the importance of considering the effects of load related bottom deformations in tidal models, since even if their contribution to the tidal patterns might be small it is clear that their effect over the dissipation of the available tidal energy is not necessarily small. The disregard or improper representation of the tidal load effects might require the introduction of unrealistically large bottom friction coefficient parameterization.

Based on observations, Candela *et al.* (1990) obtained a net M_2 tidal energy flux at Gibraltar of 8 10^8 W. However, their estimated observational error was an order of magnitude larger ~10^9 W. Without further evidence, they concluded that there was no discernible net energy flux through the Strait – a conclusion which should now be reconsidered in view of the results presented here.

Semi-enclosed basin normal modes

The reduced dynamic system chosen for the analysis of the M_2 tide in this paper resolves 228 normal modes for the Mediterranean Sea. The projection of the complete solution for the M_2 tide in the Mediterranean (Fig. 5) on to these modes gives the normal mode constituency of the M_2 tide in the basin. This is shown in Figure 8*a* where the percentage of variance of the tide represented by each mode in the projection is plotted with respect to an arbitrary mode number. The mode projection coefficients (27) are decomposed as $a_n = f_f f_s$; where the factor $f_f = i/\omega - \omega_n$, depends on the difference between the tidal and mode frequencies and a spatial structure dependent factor $f_s = \dfrac{Y'_{ln} U^{-\frac{1}{2}} f}{Y'_{ln} Y_{rn}}$.

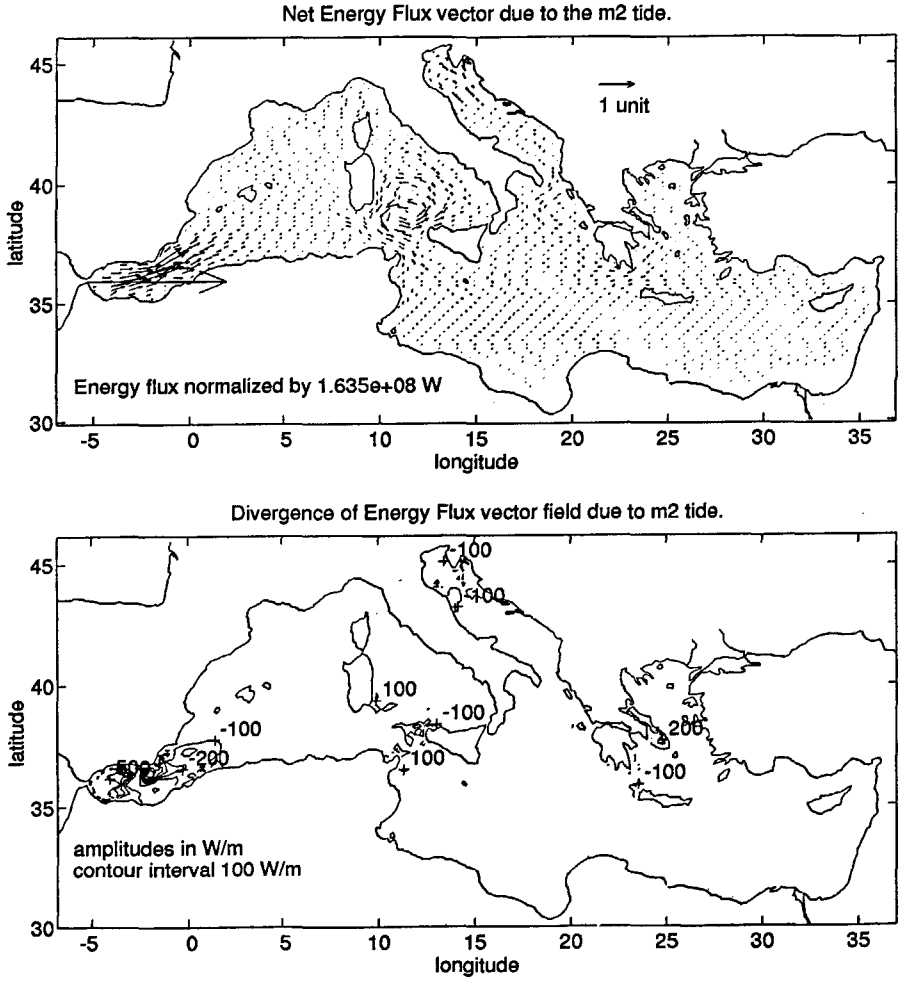

Figure 7

Net energy flux vector due to the M_2 tide (upper panel). The vectors in the interior of the Sea and in the Strait of Gibraltar are normalized by the value of 1.6 10^8 W which corresponds to the unit scale indicated in the upper right-hand corner of the panel. Energy flux divergence in W/m (lower panel). Negative values indicate areas where tidal energy converges.

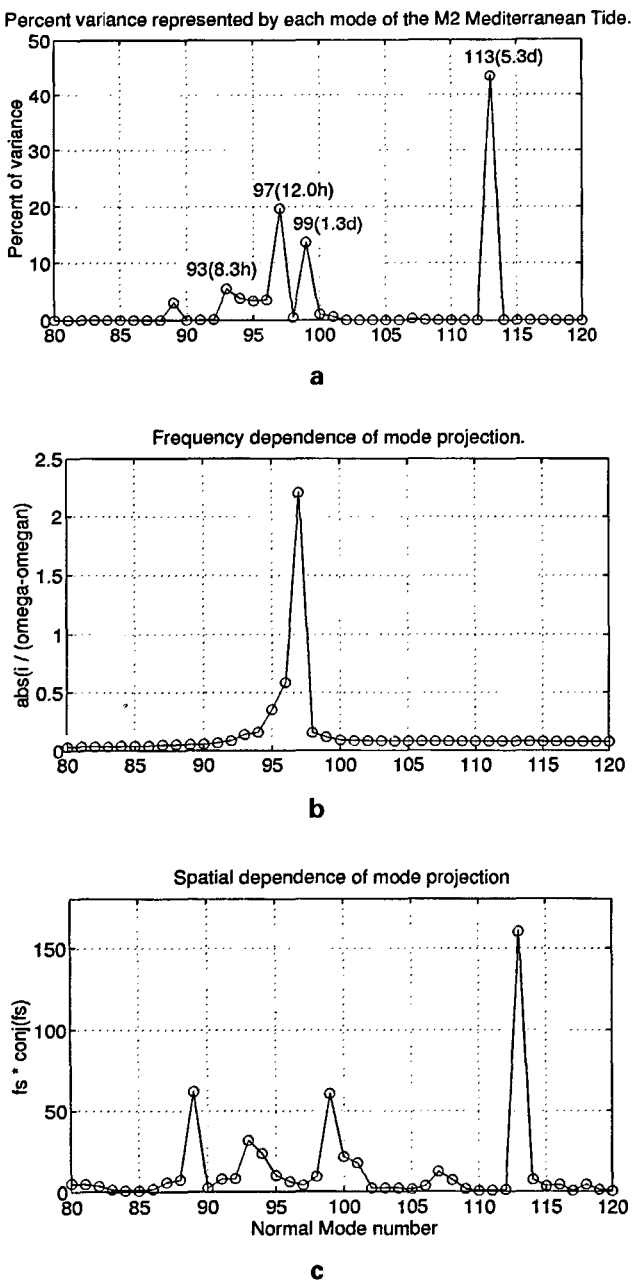

Figure 8

Projection of the tidal solution shown in Figure 5 on to the normal modes resolved for the basin. The percentage of variance represented by each of the modes is plotted with respect to an arbitrary mode number assignment. The four most relevant modes in the representation are indicated by their number followed by their corresponding period. Temporal (b) and spatial (c) dependence of the tidal solution projection on to the basin modes. In both (b) and (c) an arbitrary amplitude is plotted vs. *mode number.*

A given mode can make an appreciable contribution to the projection either by having a natural frequency close to the forcing frequency or by having a spatial structure which matches that of the forcing. Figure 8 also shows plots of f_f (*b*) and f_s (*c*) which graphically explain why a given mode is excited by the specific tidal forcing.

The normal mode representation for the M_2 tide is quite efficient since eight modes represent 96 % of this tide. Four of the modes are particularly important, each contributing more than 5 % to the M_2 tide variability in the Sea. In what follows, a description of these modes is given, referring to them by their assigned number in Figure 8.

Mode 93 (Fig. 9) is a gravitational mode, as the ratio of potential to kinetic energy (pe/ke = 1.001) indicates. It has a period of 8.3 h and a maximum sea surface elevation amplitude in the Gulf of Gabes. This is a very active mode throughout the whole Sea with important water exchanges between the Tyrrhenian and Algerian basins in the Western Mediterranean and between the Ionian and Levantine basins in the Eastern Mediterranean.

Mode 97 (Fig. 10) is also gravitational (pe/ke = 0.99) with a period of 12.03 h. This mode has the period closest to the M_2 tide period (12.42 h). The sea surface elevation shows maximum amplitudes at the head of the Aegean Sea. Large amplitudes are also observed at the head of the Adriatic Sea where it forms the characteristic amphidromic point of the semi-diurnal tides described in earlier work (Hendershott and Speranza, 1971). This mode has its main activity concentrated in the Eastern Mediterranean, implying important transports between the Adriatic, Ionian, Aegean and Levantine basins.

Mode 99 (Fig. 11) is a mixed mode (pe/ke = 0.69) and has a period of 1.3 day. This mode accounts for the energy exchanges between the Western and Eastern Basins through the Strait of Sicily, where it forms a sea surface amphidromic point. This mode also implies appreciable flows through the Strait of Gibraltar.

Mode 113 (Fig. 12) has a periodicity of 5.3 days and corresponds to the Helmholtz mode of oscillation between the Mediterranean Sea and the North Atlantic Ocean due to the opening at the Strait of Gibraltar. Even though its period is quite distant from that of the M_2 tide its spatial structure matches that of the co-oscillating tide being forced by the Atlantic Ocean, which actually drives this mode at the M_2 tidal period.

Comparison with tidal gauges

The available tidal information consisted of about 100 tide gauge constants compiled by the International Hydrographic Organization (1979). In order to compare the data with the model it is desirable to have an adequate estimate of the error in the observations and the ability to eliminate local effects. This quality control work was not done due to the lack of sufficient information. Instead a selection of 60 tidal stations shown in Figure 13*a* distributed over the entire basin was made. In the process of selection, the stations in the Gulf of Gabes were deliberately eliminated, since the ETOPO5 bathymetry data around this area are not reliable. Other stations eliminated included stations with contradictory values in the Adriatic, and stations in the Strait of Messina.

Using these 60 stations in the assimilation algorithm, described at the end of the "Methods" section, and as a norm the root mean squared distance between the model and the observations, we find the following results.

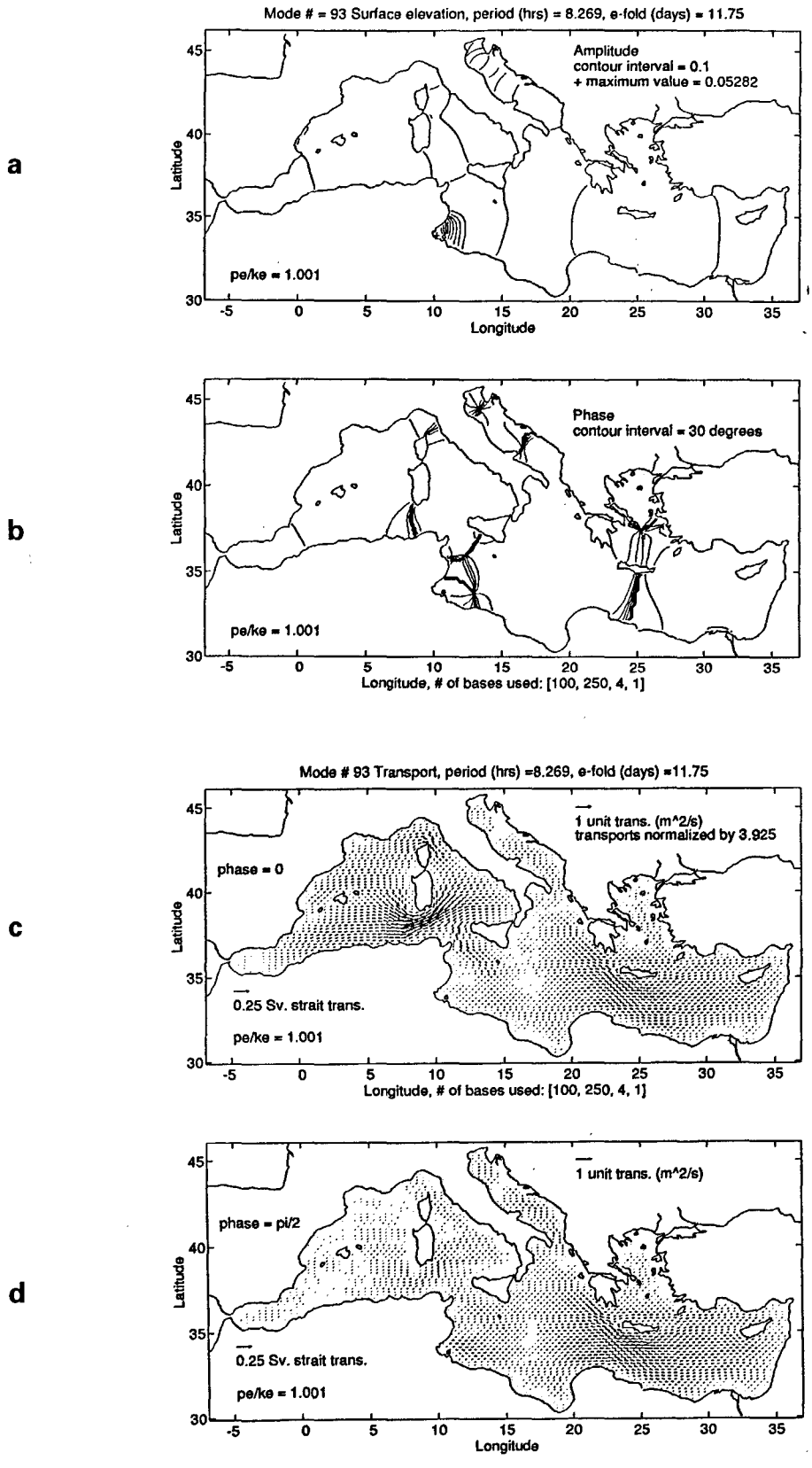

Figure 9

Normal mode 93. (a) Sea surface amplitude contours normalized by the maximum value indicated in the upper right-hand corner. The ratio of potential to kinetic energy (pe/ke) is also indicated. (b) Contours of constant sea surface elevation phase in degrees. (c) Transports at phase zero and (d) a quarter of a cycle later. All transport in the interior of the Sea are in m^2/s, normalized and scaled by the value given in the upper right hand corner of panel (c). The transport through the Strait of Gibraltar are in Sverdrups with the scale shown. Magnitudes of the sea surface elevation, interior transports and transports through the Strait are relative to each other but arbitrary.

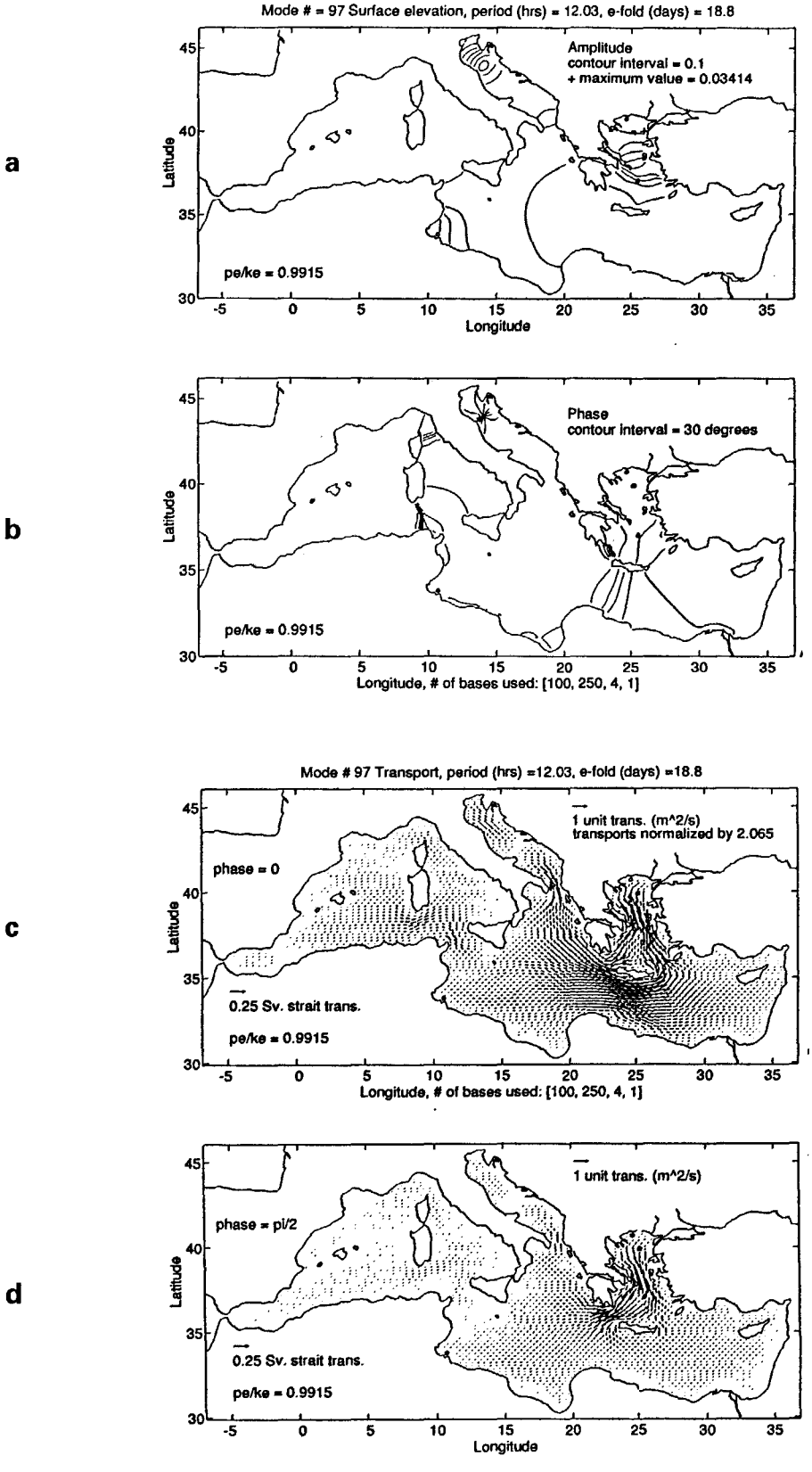

Figure 10

Normal mode 97. (a) Sea surface amplitude contours normalized by the maximum value indicated in the upper right-hand corner. The ratio of potential to kinetic energy (pe/ke) is also indicated. (b) Contours of constant sea surface elevation phase in degrees. (c) Transports at phase zero and (d) at a quarter of a cycle later. All transport in the interior of the Sea are in m^2/s, normalized and scaled by the value given in the upper right-hand corner of panel (c). The transport through the Strait of Gibraltar are in Sverdrups with the scale shown.

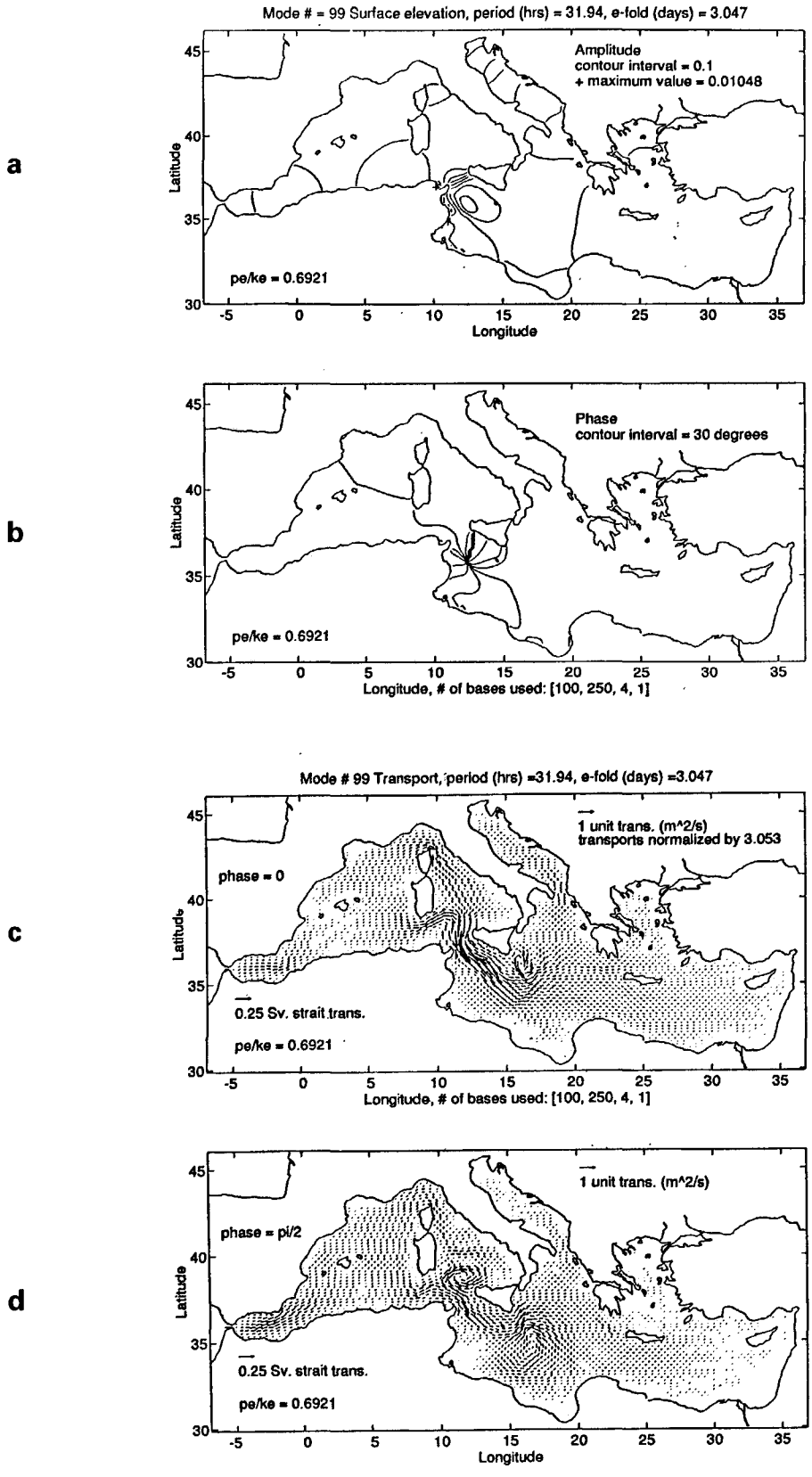

Figure 11

Normal mode 99. (a) Sea surface amplitude contours normalized by the maximum value indicated in the upper right hand corner. The ratio of potential to kinetic energy (pe/ke) is also indicated. (b) Contours of constant sea surface elevation phase in degrees. (c) Transports at phase zero and (d) at a quarter of a cycle later. All transport in the interior of the Sea are in m^2/s, normalized and scaled by the value given in the upper right-hand corner of panel (c). The transport through the Strait of Gibraltar are in Sverdrups with the scale shown.

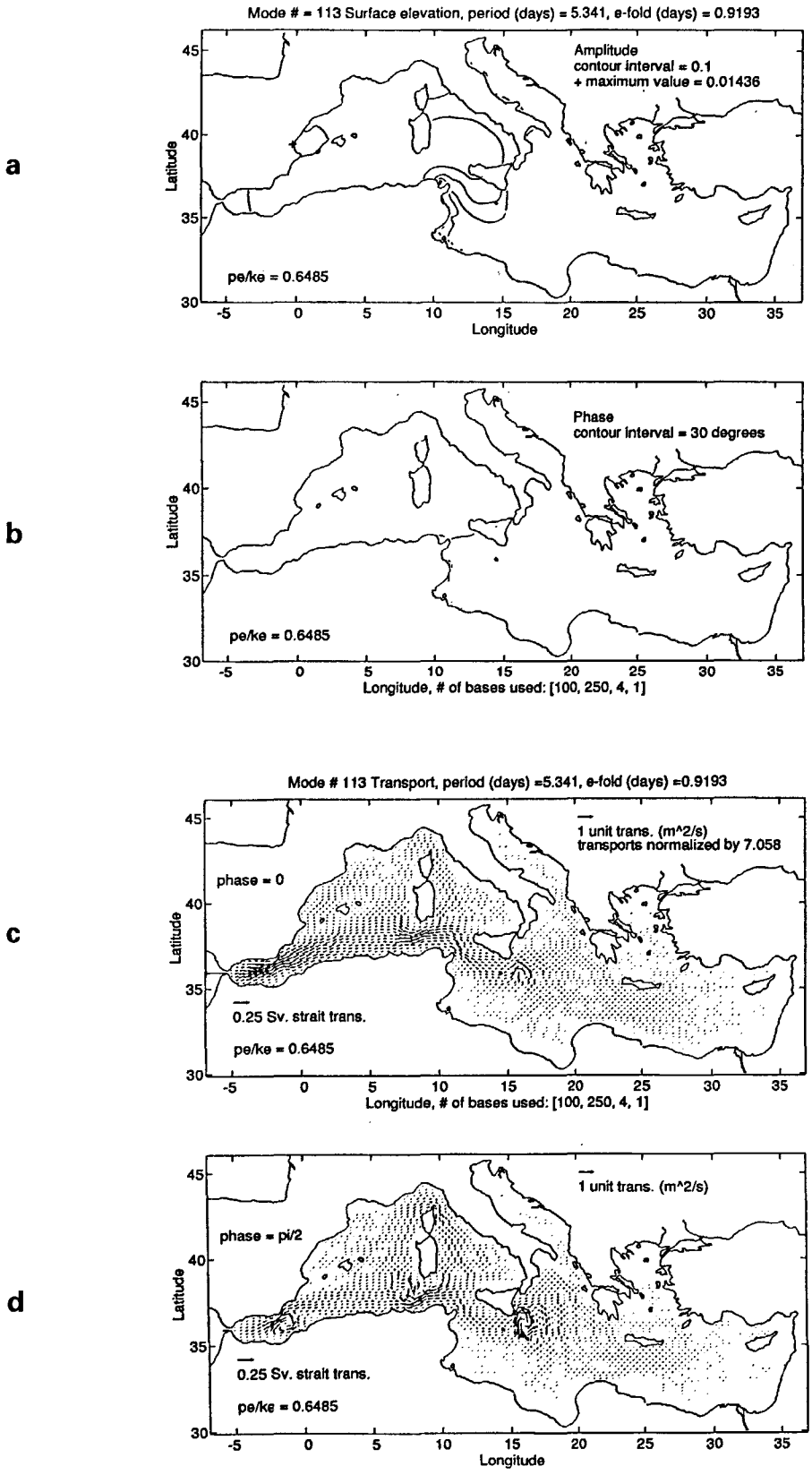

Figure 12

Normal mode 113. (a) Sea surface amplitude contours normalized by the maximum value indicated in the upper right-hand corner. The ratio of potential to kinetic energy (pe/ke) is also indicated. (b) Contours of constant sea surface elevation phase in degrees. (c) Transports at phase zero and (d) a quarter of a cycle later. All transports in the interior of the Sea are in m^2/s, normalized and scaled by the value given in the upper right-hand corner of panel (c). The transports through the Strait of Gibraltar are in Sverdrups with the scale shown.

a

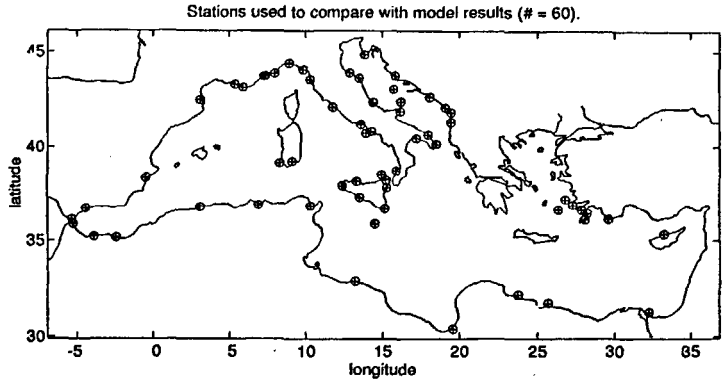

b

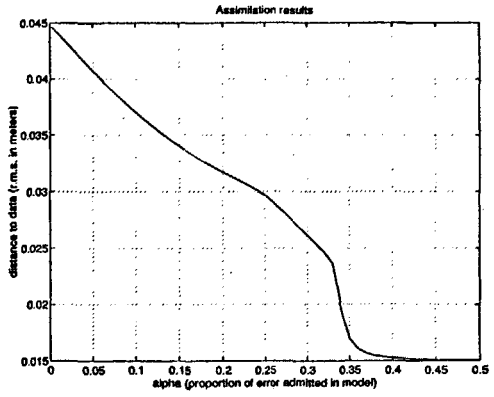

c

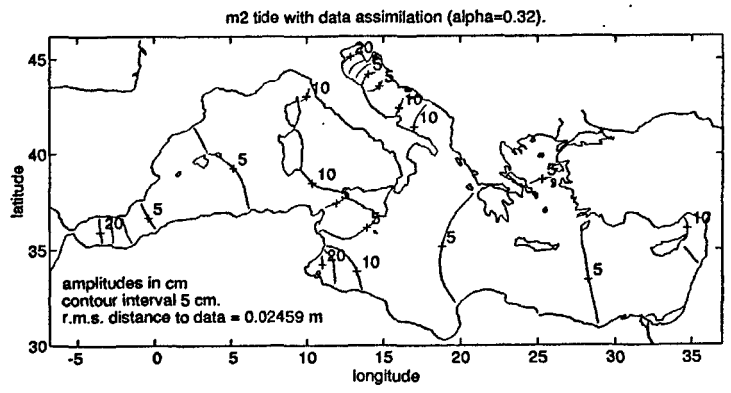

d

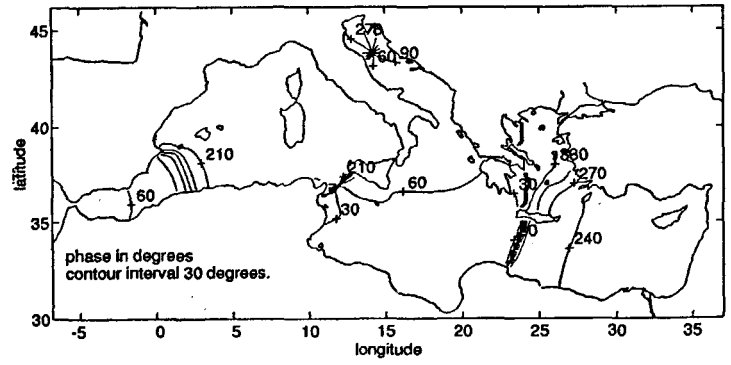

Figure 13

(a) Location of the 60 stations used to compare the model results. (b) Plot of the distance between the model results and the observations, i.e. $(d'd)^{1/2}$/(number of observation points), as a function of α (equation 39) that gives the proportion of error allowed in the model. (c) Sea surface elevation amplitude and phase (d) contours for the solution corresponding to $\alpha = 0.32$.

Figure 13*b* shows the magnitude of the data residual norm as a function of a defined in (39), *i.e.* the proportion error allowed in the model. For a = 0 the data is ignored, and the magnitude of the residual norm associated to the model is $| d_m | \sim 4.5$ cm. The non-observable portion of the data has a magnitude $| \tilde{d}_m | = 1.51$ cm, corresponding to values of α higher than 0.45. This implies that the best possible fit to the data requires a deviation s of about 45 % in size of the model solution $\mathbf{y}_M$. The tidal amplitude associated with this solution (not shown here) contains unrealistic small-scale patterns. An intermediary solution, allowing a deviation of 32 % from the model solution and with data residual of 2.5 cm is shown in Figures 13*c* and 13*d*. In this case the patterns of the sea surface height are relatively close to those of the unconstrained model solution (Fig. 5).

At this point it would be possible to proceed further and explore the effects of the assimilation on the currents, forcings, *etc.* This avenue is not pursued here since the results suggest that the tidal gauge data available to us do not provide the quantity and quality of data required for the melding of data and dynamics sought in the present study.

DISCUSSION AND CONCLUSIONS

The tidal response of a semi-enclosed basin, such as the Mediterranean Sea is properly described in terms of the normal modes of the semi-enclosed basin, as distinguished from those related to a closed basin. The definition of the semi-enclosed modes followed explicitly here is that associated with the classical split of the tidal response into a co-oscillating and independent tide. In other words, the semi-enclosed mode is defined by a zero amplitude in the Atlantic Ocean. An alternative is to consider the scattering problem, that is, including the radiation of the tide into the Atlantic. We have carried out the computations including the radiation terms (not shown here), and we have found that the radiation load is not significant (4 cm of amplitude in the Gulf of Cadiz); thus we have opted to maintain the traditional approach here, noting nonetheless that, if the radiation load is significant, the scattering problem formulation is more satisfactory. The importance of the normal modes is that the tide can be understood using a few degrees of freedom and permits us to identify separately the sensitivity to the spatial and temporal components of the forcings. This is intimately related to the use of admittance to identify basin modes (Platzman, 1991).

The co-oscillating and independent tides interference leads to the interesting situation in which the independent tidal forcing extracts energy from the system. In addition to the independent tide, bottom dissipation and tidal load effects extract energy from the system. Bottom dissipation extracts energy regardless of flow configuration; and we have shown that the *local* tidal load is also dissipative for sufficiently small basins, including the Mediterranean Sea. The fact that the *global* tidal load is extracting energy is peculiar to the given flow pattern of the Sea. The *local* ocean tidal load contributes in two ways to the dynamics of the basin. The first, like the *global* tidal load, transmits energy to the lithosphere. The second is as an interaction between the sea surface height and the irrotational transport component. The latter is not significant; whereas the dissipative part is comparable to bottom friction, indicating that despite its apparent smallness it influences the overall response since it is a significant contribution to the Q of the system.

In the course of the present study, it became apparent that the Strait of Gibraltar opening plays a fundamental role in determining the response of the Sea. Our simple approach to include the dynamics of the Strait (15) was justified, and known to work, based on previous analytical studies (Candela, 1991). However, it is clear that a more complete representation of the Strait's dynamics would be helful in reaching a more complete understanding of the strait-basin interaction. Possible additional physics include rotational, frictional and hydraulic effects within the Strait and the radiational load mentioned above.

The quantitative comparison with tide gauge data and the qualitative comparison with tidal currents suggest that the model estimate, unconstrained by the data, gives satisfactory initial results. There remain some deficiencies made apparent using tide gauge data. These include an underestimate of the tides in the Gulf of Gabes and overestimate of the tides in the Adriatic. Some of these deficiencies are related to the fact that, in the model discretization, the metric terms associated to the sphericity of the Earth were not included, and – in the case of the Gulf of Gabes – to poor resolution of the bathymetry. A further consideration, when comparing model and data, is that for coastal stations there is a difference in position between the actual location of the tide observation and the closest model node where the predictions are made. In order properly to take into account this situation, it is necessary to study the geographical location of each station with respect to the nearest model node and, for each individual case, to construct the appropriate transfer function for extrapolating the model prediction to the station location or *vice-versa*. Until these transfer functions are constructed for the coastal stations used, the model-data comparison will have a degree of arbitrariness. Tide gauge data are not in themselves sufficient to verify the dynamics, even with the assumption that they have negligible errors. The TOPEX-POSEIDON data set and an increased current data set will improve our ability to close the gap in this direction.

Acknowledgements

Helpful comments from Professor George W. Platzman and an anonymous reviewer are gratefully acknowledged. This work was supported by ONR grant N00014-93-1-0415. This is Woods Hole Oceanographic Institution contribution number 8770.

REFERENCES

Albérola C., S. Rousseau, C. Millot, M. Astraldi, J. Font, J. Garcia-Lafuente, G.P. Gasparini, U. Send, A. Vangriesheim (1995). Tidal currents in Western Mediterranean Sea. *Oceanologica Acta* **18**, 2, 273-284.

Alterman Z., H. Jarosch, C.L. Pekeris (1959). Oscillations of the *Earth. Proc. Royal Soc. London A*, **252**, 80-95.

Accad, Y., C.L. Pekeris (1978). Solution of the tidal equations for the M_2 and S_2 tides in the world oceans from a knowledge of the tidal potential alone. *Proc. Royal Soc. London, A*, **290**, 235-266.

Canceill, P., R. Agelou, P. Vincent (1994). Barotropic tides in the Mediterrenean Sea from a finite element numerical model. Submitted to *J. Geophys. Res. Oceans.*

Candela J. (1991). The Gibraltar Strait and its role in the dynamics of the Mediterranean Sea. *Dyn. Atmos. Oceans* **15**, 3-5, 267-300.

Candela J., C.J. Lozano (1994). Barotropic response of the western Mediterranean to observed atmospheric pressure forcing, In: *The Seasonal and Interannual Variability of the Western Mediterranean Sea*, Paul La Violette, ed. Coastal and Estuarine Studies, **46**, 325-359. American Geophysical Union.

Candela J., C.D. Winant, A. Ruiz (1990). Tides in the Strait of Gibraltar. *J. Geophys. Res.* **95**, 7313-7335.

Carrier G.F., R.P. Shaw, M. Miyata (1971). The response of narrow-mouthed harbors in a straight coastline to periodic incident waves. *J. App. Mech.* June, 335-344.

Cartwright D. E., R.D. Ray (1990). Oceanic tides from Geosat altimetry. *J. Geophys. Res.* **95**, 3069-3090.

Defant A. (1961). *Physical Oceanography*, **2**, Pergamon Press, Oxford, 598 p.

Dressler R. (1980). Hydrodynamisch-nümerische Untersuchungen der M_2 Gezeit und einiger Tsunamis im europäischen Mittenmeer. *Mitteilungen Inst. für Meereskunke*, Universität Hamburg, Hamburg, 30 p.

Elliott AJ. (1993). Waves, Tides and surges in the Mediterranean, in: *Mediterranean Sea Volume II*, Eds. A.C. and A. Robinson, Reports in Meteorology and Oceanography, Harvard University, Cambridge Massachusetts, **45**, 330 p.

Farrell W.E. (1972). Deformation of the Earth by Surface Loads. Rev. *Geo-phys. and Space Phys.* **10**, 761-797.

Francis O., P. Mazzega (1990). Global Charts of Ocean Tide Load Effects. *J. Geophys. Res.* **95**, C7, **11**, 411-11, 424.

Grace S.F. (1931). Historical review of dynamical explanations of the tides in the Mediterranean Sea, the Baltic Sea, the Gulf of Mexico and the Arctic Ocean, *Publ. Scientifique. Assoc. d'Océanographie Physique* **1**, 15-26.

Godin G. (1988). Tides, CICESE, Ensenada, Baja California, México, 290 p.

Hendershott M.C. (1972). The Effects of Solid Earth Deformation on Global Ocean Tides. Geophys. *J. R. Astr. Soc.* **29**, 389-402.

Hendershott M.C., A. Speranza (1971). Co-oscillating tides in long, narrow bays; The Taylor problem revisited. *Deep-Sea Res.* **18**, 959-980.

International Hydrographic Organization (1979). Tidal constituent bank. Station Catalogue, Ocean and Aquatic Sciences, *Dept. of Fisheries and Oceans*, Ottawa.

Lacombe H. (1961). Contribution à l'étude du régime du détroit de Gibraltar *Cah. Océanogr.* **13**, 73-107.

Liveriatos E., M. Zadro (1977). A study of the hydrodynamic behavior of the Aegean basin. *Boll. Geof. Teor. ed Appl.* **19**, 179-198.

Maloney W.E., R.E. Burns (1958). A reppraisal of the tides of the Mediterranean. *U.S. Navy Hydrographic Office*, Technical Report 61, Washington DC, 32 p.

Molines J. (1991). Modelling the barotropic tides in the Strait of Sicily and Tunisian Shelf. *Oceanologica Acta* **14**, 241-252.

Mosseti F. (1989). Marées et courants de marées en trois régions cruciales de la mer Méditerranée: mesures et modèles. *Boll. Di Ocean. Teor. ed Appl.* **8**, 123-134.

Mosseti F., N. Purga (1989). The semi-diurnal tides in the Sicily Straits. *Il Nuovo Cimento* **12c**, 349-355.

Platzman G.W. (1972). Two dimensional free oscillations in natural basins. *J. Phys Oceanogr.* **2**, 117-138.

Platzman G.W. (1978). Normal modes of the world ocean. Part I: Design of a finite-element barotropic model. *J. Phys. Oceanogr.* **8**, 323-343.

Platzman G.W. (1979). Effects of multiple connectivity on a finite-element baratropic model. *J. Phys. Oceanogr.* **9**, 1276-1283.

Platzman G.W. (1991). Tidal Evidence for Ocean Normal Modes. In "Tidal Hydrodynamics", edited by B. B. Parker. John Wiley and Sons, Inc. 883 p.

Proudman J. (1938). On a general expansion in the theory of tides. *Proc. London Math. Soc.* **29**, 527-536.

Purga N., F. Mosetti, E. Acerboni (1979). Tidal harmonic constants for some Mediterranean harbors. *Boll. Geof. Teor. ed Appl.* **21**, 72-81.

Sanchez B.V., R.D. Ray, D.E. Cartwright (1992). A Proudman-function expansion of the M_2 tide in the Mediterranean Sea from satellite altimetry and coastal gauges. *Oceanologica Acta* **15**, 325-337.

Schwab D.J., D.B. Rao (1983). Barotropic oscillations of the Mediterranean and Adriatic Seas. *Tellus* **35A**, 417-427.

Tikhonov A.N., V.Y. Arsenin (1977). *Solution of Ill-posed Problems*. W. H. Winston and Sons, Washington, D.C.

Villain M.C. (1949). Sur la marée à Alger et en Méditerranée occidentale, C.O.E.C. *Bull. d'Information* **4**, 92-103.

Villain M.C. (1952). Les Marées de la Méditerranée orientale, C.O.E.C., *Bull. d'Information* **4**, 92-103.